



# RESEARCH MEMORANDUM

ALTITUDE INVESTIGATION OF SEVERAL AFTERBURNER  
CONFIGURATIONS FOR THE J40-WE-8 TURBOJET ENGINE

By E. William Conrad and Carl E. Campbell

Lewis Flight Propulsion Laboratory  
Cleveland, Ohio

NATIONAL ADVISORY COMMITTEE  
FOR AERONAUTICS  
WASHINGTON

July 16, 1953  
Declassified September 29, 1960

## NATIONAL ADVISORY COMMITTEE FOR AERONAUTICS

RESEARCH MEMORANDUMALTITUDE INVESTIGATION OF SEVERAL AFTERBURNER CONFIGURATIONS  
FOR THE J40-WE-8 TURBOJET ENGINE

By E. William Conrad and Carl E. Campbell

## SUMMARY

An investigation was conducted in the Lewis altitude wind tunnel to evaluate the performance and operational characteristics of the J40-WE-8 afterburner. Although the minimum afterburner-inlet pressure which would occur within the specified operating envelope of the engine was 730 pounds per square foot, stable operation was desired at a lower pressure to provide a "safety margin." Since the combustion efficiency was low at the chosen burner-inlet pressure of 620 pounds per square foot, a brief program of modifications was undertaken wherein the changes in configuration were restricted by production considerations.

Modifications were made to the flame holder, the diffuser, and the fuel system. Inasmuch as the peak combustion efficiency of the original configuration was 0.90 or higher at burner-inlet pressures of 1500 pounds per square foot or higher, no appreciable improvement was possible. At a pressure of 620 pounds per square foot, the peak efficiency was raised only slightly (from 0.47 to 0.54) by the modifications to the configuration. Over most of the range of fuel-air ratios, the combustion efficiency was increased about 0.17 at the lower pressure level. This increase resulted in an increase in the maximum exhaust-gas temperature from 2380° to about 2950° R, an increase in maximum net thrust from 1500 to 1660 pounds, and a reduction in specific fuel consumption at stoichiometric fuel-air ratio (0.067) from 3.70 to 3.15 pounds of fuel per hour per pound of net thrust. The configuration giving the best performance was, however, subject to buzzing combustion under certain operating conditions.

## INTRODUCTION

An investigation was conducted in the NACA Lewis altitude wind tunnel to determine the altitude performance and operational characteristics of an afterburner developed by the manufacturer for the J40-WE-8 turbojet engine. This afterburner configuration evolved from a development program conducted by the engine manufacturer at sea-level static conditions. Because the manufacturer's scheduled production of the afterburner had been started, the changes made during this study to improve the altitude performance were restricted to modifications which would introduce no appreciable production delay. As a result, several modifications which

appeared to be desirable on the basis of previous investigations were not made in the phase of the program reported herein.

The original configuration supplied by the manufacturer incorporated several design features which had been found to eliminate screeching (high frequency) combustion instability. During the study reported herein, changes were made in the fuel-injection system to improve the fuel-air distribution and fuel mixing length; in the diffuser configuration to improve diffuser velocity profiles; and in the flame holder to improve flame propagation between the two rings. Each configuration was also investigated with respect to operation, primarily to detect the presence of screech.

Performance data for several configurations are shown for a range of afterburner fuel-air ratios at altitudes from 10,000 to 45,000 feet and flight Mach numbers from 0.18 to 0.78, corresponding to afterburner-inlet pressures from 2750 to 620 pounds per square foot absolute.

#### APPARATUS AND INSTRUMENTATION

The engine used in this investigation is designated "the prototype J40-WE-8 engine." The static sea-level thrust of this engine without afterburner is about 7500 pounds at an engine speed of 7260 rpm and an average turbine-inlet temperature of 1425° F.

Main components of the engine (fig. 1) include an 11-stage axial-flow compressor, a single-annular combustor, a two-stage turbine, a diffuser assembly, an afterburner combustion chamber, a continuously variable clam-shell-type exhaust nozzle, and an electronic control. During afterburner operation, the variable-area exhaust nozzle was actuated by the control to maintain limiting turbine-inlet temperature over the full range of afterburner fuel-air ratios. The over-all length of the engine is 284 inches, the maximum diameter is 45.5 inches, and the total weight is approximately 3560 pounds.

#### Installation

The engine was mounted on a wing that spanned the 20-foot-diameter test section of the altitude wind tunnel. Engine inlet-air pressures corresponding to altitude flight conditions were obtained by introducing dry refrigerated air from the tunnel make-up air system through a duct to the engine inlet. A slip joint with a frictionless seal was used in the duct, thereby making possible the measurement of thrust and installation drag with the tunnel scales. Air was throttled from approximately sea-level pressure to the desired pressure at the engine inlet, while the static pressure in the tunnel test section was maintained to correspond to the desired altitude.

### Instrumentation

Instrumentation for measuring pressures and temperatures was installed at several stations throughout the engine and afterburner as indicated in figure 2. Air flow was determined from pressure and temperature measurements at the turbine inlet and outlet as discussed in the appendix. A traverse mechanism comprising 10 sonic-type thermocouples was supplied by the engine manufacturer to determine the gas-temperature pattern at the turbine inlet. A comprehensive pressure and temperature survey was obtained at the turbine outlet, station 6. Diffuser-outlet pressures were determined by a single rake of total-pressure tubes spanning the diameter of the diffuser exit at station 7. Total and static pressures several inches upstream of the exhaust-nozzle outlet were measured by means of a water-cooled survey rake which was so mounted that the rake drag could be measured by a pneumatic capsule. The symbols and methods of calculation used in this report are given in the appendix.

### Afterburner Designs

A sketch of the afterburner shell with pertinent dimensions is shown in figure 3. This shell was common to all configurations. Cooling of the afterburner shell was accomplished by passing compressor bleed air through the annular passage formed between the shell and the concentric shroud. The production diffuser geometry was changed for one configuration as shown by the sketches and photographs of figure 4. The production configuration and the annular cascade diffuser are shown in figures 4(a) and 4(b), respectively. The annular cascade diffuser was designed to produce uniform velocity distribution at the flame holder.

The two flame holders used during this study are shown in figure 5. These flame holders consisted of two annular V-gutters with mean diameters of 17 and  $29\frac{1}{2}$  inches and incorporated longitudinal T-shaped stringers 1 inch wide, which were devised by the engine manufacturer to avoid screeching combustion. The flame holder shown in figure 5(b) differed from that of figure 5(a), in that outer gutters were joined by cross gutters  $1\frac{7}{8}$  inches wide in lieu of stringers, in order to aid in flame propagation between gutters. Blockages were 41.3 and 38 percent of the combustion-chamber cross-sectional area for flame holders A and C, respectively. The photograph in figure 5 shows the louvers in the flame-holder leading edges which were used for all but one configuration.

The two fuel-distribution patterns used are shown in figure 6. Fuel was injected through simple orifices. Each of the three fuel-manifold rings (fig. 6(a)) was connected to a separate throttle to permit individual regulation of the fuel flow. With the five-ring fuel manifold of

figure 6(b), one throttle was used to govern the flow of the inner three rings, while a separate throttle was used with each of the outer rings. Throughout most of the program, the fuel orifice diameter was 0.041 inch. The three-ring manifold of figure 6(a) was modified for some configurations by reducing the hole size to 0.027.

The components described in the previous paragraphs were used in various combinations. The combinations of these components and the details of fuel-injection location and direction of fuel spray are summarized in table I. The individual configurations are described briefly in the following paragraphs:

Configuration A. - Configuration A was the original design supplied by the manufacturer. It comprised the diffuser inner cone shown in figures 4(a) and 4(d), the flame holder and fuel manifold assembly shown in figure 5(a), and the fuel-injection pattern shown in figure 6(a). The fuel from all three manifolds was injected in a downstream direction, and the manifolds were  $1\frac{1}{2}$  inches upstream of the flame holder. Every alternate hole in the fuel-injection manifold was in line with a louver in the leading edge of the flame-holder gutters.

Configuration B. - Configuration B was identical to configuration A, except that louvers in the flame holder were covered.

Configuration C. - Configuration C was identical to configuration A, except that the flame stabilizing bars between the two annular gutters were replaced by eight radial V-gutters.

Configuration D. - Configuration D differed from configuration A in two respects: the annular cascade shown in figure 4(c) was installed in the diffuser (fig. 4(b)), and the five-ring fuel manifold of figure 6(b) was installed.

Configuration E. - Configuration E was identical to configuration A, except that the fuel was injected in an upstream direction from the inner and outer fuel rings to increase the time for fuel droplet vaporization.

Configuration F. - Configuration F differed from configuration A only in that the outer fuel manifold was moved  $8\frac{1}{4}$  inches upstream to allow more time for fuel droplet vaporization.

Configuration G. - Configuration G was the same as configuration F, except that the fuel from the outer fuel ring was sprayed in an upstream direction, with alternate holes drilled  $10^\circ$  outward and  $30^\circ$  inward from an axial direction. This stagger in the holes was made to allow for possible misalignment of the fuel with respect to the outer gutter.

Configuration H. - Configuration H differed from configuration G in that all fuel holes were reduced from 0.041- to 0.027-inch diameter and a fourth ring (inoperative) was added where the outer ring was removed in configuration F.

Configuration I. - Configuration I was the same as configuration H, except the holes in the outer fuel ring were drilled 5° outward and 5° inward from axial.

#### PROCEDURE

Throughout the afterburning program, the electronic control maintained an engine speed of 7260 rpm (rated speed) and a turbine-inlet temperature of approximately 1425° F. The afterburner-inlet conditions of pressure, temperature, and velocity were therefore nearly constant at each particular flight condition. The four simulated flight conditions at which performance data were obtained are shown in the following table:

Altitude, ft	Flight Mach number	Average burner- inlet total pressure, lb/sq ft	Configuration								
			A	B	C	D	E	F	G	H	I
10,000	0.18	2750	✓		✓		✓	✓		✓	✓
20,000	.78	2600	✓	✓	✓		✓	✓		✓	✓
35,000	.78	1500	✓	✓	✓	✓	✓	✓	✓	✓	✓
45,000	.18	620	✓	✓			✓		✓	✓	✓

The lowest altitude of 10,000 feet is a facility limit and corresponds to an afterburner-inlet pressure of 2750 pounds per square foot. The data at 45,000 feet correspond to a total pressure of 620 pounds per square foot absolute at the afterburner inlet. Although this pressure is slightly lower than the minimum given in the engine specifications (approximately 730 lb/sq ft), adequate performance at the lower pressure was desired to provide a "margin of safety." The data at the intermediate altitudes were used to obtain performance at flight speeds within the normal flight envelope of most airplanes. Because of facility limitations, the data at 10,000 and 45,000 feet could not be obtained at simulated flight Mach numbers above 0.18. As shown in the preceding table, data were not obtained at all four conditions with all configurations. Only enough data were obtained to indicate the relative merit of each configuration. At the 35,000-foot flight condition, variations were made in the three throttles governing the fuel distribution to obtain the optimum performance. Comparison of configurations are made on the basis of the optimum fuel balance for each.

For each flight condition, except where limited by available time, data were obtained over a range of afterburner fuel-air ratios from the lean blow-out limit to a maximum value determined by (a) maximum exhaust-nozzle area, (b) maximum allowable fuel pressure, (c) rich blow-out, or (d) screeching combustion. Screeching combustion (refs. 1 and 2) is a type of combustion instability characterized by severe pressure pulsations having a frequency of 600 to about 6000 cycles per second.

## RESULTS AND DISCUSSION

### Afterburner Performance

Afterburner-inlet conditions. - The afterburner-inlet conditions of total pressure, total temperature, and velocity obtained with several configurations at the various flight conditions are shown in figure 7 as a function of afterburner fuel-air ratio. Inasmuch as the inlet conditions are not influenced by changes in the afterburner configurations, the average values shown in figure 7 apply to all the configurations discussed herein. The average values of turbine-outlet total pressure (fig. 7(a)) for the four flight conditions investigated varied from approximately 2750 to 620 pounds per square foot absolute with a maximum deviation of  $\pm 6$  percent. In accordance with a previously determined relation between turbine-inlet and turbine-outlet temperature, the outlet temperature was allowed to vary with flight conditions as shown in figure 7(b) in order to give limiting turbine-inlet temperature of about  $1885^{\circ}$  R at all conditions. The average turbine-outlet temperature thus varied from approximately  $1500^{\circ}$  R at a turbine-outlet pressure level of 2750 pounds per square foot absolute to about  $1600^{\circ}$  R at a pressure level of 620 pounds per square foot absolute. Average velocities at the flame holder ranged from about 300 to 400 feet per second for all the configurations investigated, as shown in figure 7(c). Although the average velocities did not vary appreciably with changes in configuration, the radial velocity distribution at the flame holder was altered by a change in diffuser configuration as shown in figure 8. The high velocity peak in the region of the flame-holder gutters with configuration A was reduced considerably by installing deflector vanes (figs. 4(b) and 4(c)) in the diffuser for configuration D. With the exception of configuration D, all configurations had the same diffuser and velocity profile as configuration A.

Pressure-loss characteristics. - The total-pressure-loss ratio through the diffuser and the over-all total-pressure-loss ratio through the afterburner obtained with configurations A and D at an inlet pressure of 1500 pounds per square foot absolute are shown in figure 9 as functions of exhaust-gas total temperature. Installation of the deflector vanes in the diffuser (configuration D) resulted in a diffuser pressure-loss ratio of 0.07 as compared to 0.04 with configuration A. The over-all total-pressure-loss ratios, which include the friction pressure losses

across the diffuser, fuel manifold rings, and flame holder, and the momentum pressure losses due to burning are compared in figure 9(b) for these two configurations. Although the diffuser pressure loss was 3 percent higher for configuration D than for A, and an additional friction loss across the two additional fuel manifolds of configuration D would be expected, the over-all total-pressure-loss ratio was only 2 to 2.5 percent higher for configuration D than for A. This difference in losses may be attributed to the lower velocity across the flame-holder gutters of configuration D and possibly a lower momentum pressure loss with the uniform velocity distribution. The 2 or 2.5 percent higher over-all pressure loss with configuration D, however, is a disadvantage to be considered in the final comparison of configurations. With the exception of configuration D, all configurations had the same diffuser and over-all pressure-loss characteristics as configuration A.

Fuel pressures. - The effective fuel-flow area of all fuel systems except those of configurations H and I was the same. This area for configurations A to G was chosen to allow operation at sea-level, high flight Mach number conditions without exceeding the fuel-pump pressure limitations of 300 pounds per square inch. Accordingly, at the higher altitudes, as shown in figure 10, fuel pressures were reduced to extremely low values. Fuel pressures below about 10 pounds per square inch are not considered adequate to provide satisfactory fuel-spray characteristics. At low fuel-flow rates and at the burner-inlet pressure of 620 pounds per square foot absolute, the burning was often confined to the lower portion of the combustion chamber because of a "head effect" in the fuel manifolds.

Performance of original configuration. - In figure 11 the performance of configuration A is given in plots of exhaust-gas temperature, combustion efficiency, net thrust, and over-all specific fuel consumption as functions of afterburner fuel-air ratio. The maximum exhaust-gas temperature obtained with this original configuration was  $3400^{\circ}$  R at a burner-inlet pressure of 1500 pounds per square foot absolute as shown in figure 11(a). No effort was made to obtain a design capable of higher temperatures, because the engine and afterburner were designed for temperatures no greater than  $3400^{\circ}$  R. The large data spread in this region of maximum temperature is due partly to normal data scatter and partly to the variations in fuel distribution between the three fuel manifolds that were investigated before arriving at the optimum distribution. Exhaust-gas temperatures obtained at higher burner-inlet pressures agreed with the data for 1500 pounds per square foot absolute over the range of fuel-air ratios investigated; however, data were not obtained at fuel-air ratios high enough to obtain peak temperatures at these high pressure levels, because the exhaust nozzle reached the wide-open position. At a burner-inlet pressure of 620 pounds per square foot absolute, the maximum exhaust-gas temperature was only about  $2380^{\circ}$  R because of the marked reduction in combustion efficiency as illustrated in figure 11(b).

The maximum combustion efficiency obtained at a pressure level of 620 pounds per square foot absolute was only 0.47 and occurred at a fuel-air ratio of about 0.0275. At this low pressure, burning could not be established on the outer flame-holder gutter, probably because of a combination of high velocity in the region of the outer gutter (fig. 8) and the lack of fuel mixing length. However, at lower altitudes or higher burner-inlet pressures, the flame was stably attached to the outer gutter. Peak values of combustion efficiency at the three higher pressure levels were above 0.90 and occurred at fuel-air ratios between 0.03 and 0.035. The fuel-air ratio at which these curves peak is primarily a function of the fuel-air distribution pattern. Because of the "head effect" mentioned earlier, the lower half of the burner becomes excessively rich at relatively low over-all fuel-air ratios when operating at low burner pressures (and low fuel pressures), which results in a shift in the over-all fuel-air ratios for peak efficiency to lower over-all values as the burner-inlet pressure is reduced.

It will be noted that a few data points at a burner-inlet pressure of 2750 pounds per square foot absolute are above 1.0. The absolute values of combustion efficiency are accurate only to approximately  $\pm 3$  percent, because of the great sensitivity of the calculation to inaccuracies in air-flow measurement and in the value of the velocity coefficient (see appendix). However, inasmuch as the calculation method was common for all the data, comparisons are probably valid to a somewhat greater accuracy.

Net thrust values (fig. 11(c)) increased substantially as fuel-air ratio increased, except for the data at a pressure level of 620 pounds per square foot absolute. The solid symbols at an afterburner fuel-air ratio of zero indicate the standard engine thrust for each burner-inlet pressure level. Standard engine thrust is defined as the engine thrust that would be obtained at rated speed with the standard engine tail pipe installed and with the same turbine-outlet pressures and temperatures that were encountered with afterburning (see appendix). At the lowest fuel-air ratios, some of the augmented thrust values were lower than the standard engine thrust. The thrust increase due to the slight amount of afterburning in these cases was not enough to compensate for the additional pressure losses due to installation of an afterburner. Maximum thrust of the engine with afterburning at an altitude of 10,000 feet and a flight Mach number of 0.18 (pressure, 2750 lb/sq ft abs) was about 1.42 times the standard engine thrust; while at an altitude of 45,000 feet and the same flight Mach number (pressure, 620 lb/sq ft abs) over the same fuel-air-ratio range, the maximum thrust was only about 1.14 times the standard engine thrust. This reduction in thrust augmentation at 620 pounds per square foot absolute is due to the very low exhaust-gas temperatures obtainable (fig. 11(a)).

Specific fuel consumption (fig. 11(d)) increased markedly with increasing fuel-air ratio, particularly at a pressure level of 620 pounds per square foot absolute. The specific fuel consumption of the standard engine is indicated by the solid symbols for each pressure level at an afterburner fuel-air ratio of zero. At a burner-inlet pressure of 1500 pounds per square foot absolute, the specific fuel consumption increased from about 1.50 at the minimum afterburning fuel-air ratio to about 3.00 near stoichiometric fuel-air ratio. As in the case of the exhaust-gas-temperature data, the specific fuel consumption values obtained at the higher pressure levels approximated the data for 1500 pounds per square foot absolute over the range of fuel-air ratios that were investigated. However, at a burner-inlet pressure of 620 pounds per square foot absolute, the specific fuel consumption was as high as 3.70 in the stoichiometric region because of low afterburner combustion efficiency.

Effect of modifications on combustion efficiency. - The effect on performance of alterations to the flame holder is shown in figure 12 by comparing the combustion efficiencies obtained with configurations A, B, and C. Inasmuch as the pressure-loss characteristics of these configurations did not differ appreciably, the best of these configurations with respect to combustion efficiency would also have the higher exhaust-gas temperature and net thrust and a lower specific fuel consumption. Covering the flame-holder louvers of configuration A (fig. 5(a)) to form configuration B reduced the combustion efficiency about 0.10 at a pressure level of 1500 pounds per square foot absolute. However, at the lowest pressure level, the combustion efficiency was increased as much as 0.09 in the region of peak efficiency. Elimination of the flame stabilizing members and installation of the cross gutters between the two annular gutters (configurations A and C) had no appreciable effect on performance at a pressure level of 1500 pounds per square foot absolute. Unfortunately, because of a mechanical difficulty with the ignitor, data were not obtained at the lowest pressure level where the effects of this change should have been greatest.

The effect of changing the inner and outer rings of the three-ring fuel manifold to spray upstream (configuration E) instead of downstream (configuration A) is illustrated in figure 13. At a pressure level of 1500 pounds per square foot absolute the effect of this change was negligible; however, at 620 pounds per square foot absolute the combustion efficiency was increased by as much as 0.14 as a result of the longer exposure time of the fuel droplets to the hot gas stream and the consequent improvement in fuel vaporization and distribution at the flame front. It will also be noted that, as expected, the peak combustion efficiency occurred at a higher fuel-air ratio with the less stratified mixture distribution produced by the upstream injection of configuration E.

The effects of first moving the outer fuel ring  $8\frac{1}{2}$  inches upstream (configuration F) and secondly spraying the fuel upstream from this ring with a different hole arrangement (configuration G) are shown in figure 14. Alternate fuel holes in the outer ring of configuration G sprayed the fuel  $10^\circ$  outward and  $30^\circ$  inward from an axial direction. Moving the outer fuel ring upstream decreased the efficiency somewhat at a pressure level of 1500 pounds per square foot absolute, probably because the fuel was no longer aligned with the outer gutter because of convergence or divergence of the stream lines. When upstream fuel injection from the upstream ring was used with alternate fuel jets having a radial component of flow, performance appeared to be improved at 1500 pounds per square foot absolute, and the single data point obtained at 620 pounds square foot absolute indicated an increase in combustion efficiency of approximately 0.12.

The change in fuel pressure resulting from a reduction in the size of the fuel-injection holes from 0.041-inch diameter (configuration G) to 0.027-inch diameter (configuration H) and the resulting effects on performance are shown in figures 15 and 16, respectively. For the lowest and highest common values of fuel-air ratio, the minimum fuel pressure was increased from 3 to 17 pounds per square inch, and the maximum pressure was raised from 42 to about 140 pounds per square inch, respectively, as a result of the reduction in hole size. As shown in figure 16, however, no significant effect on performance was obtained.

A review of the data showing the effects of changes made in the fuel-injection system (figs. 13, 14, and 16) shows that the effect at high burner-inlet pressures was negligible and that the efficiency at the lowest burner-inlet pressure was increased as much as 0.17 at a fuel-air ratio of 0.05. The improvement at the low pressure level was due to the establishment of stable combustion on the outer gutter of the flame holder as a result of increasing the time available for fuel evaporation and mixing.

The data thus far presented were obtained with the nonuniform air-velocity profile produced at the flame holder by the production diffuser. While a significant improvement in performance was obtained at the lowest pressure level by fuel-system modifications, the level of efficiency attained was not particularly high. It was believed that a large factor tending to limit efficiency was the high local velocity in the vicinity of the flame-holder outer gutter (fig. 8). A set of annular cascade vanes supplied by the engine manufacturer was therefore installed, reducing the velocity in the vicinity of both gutters markedly, as shown in figure 8. Simultaneously with the installation of these vanes, the five-ring fuel manifold (fig. 6(b)) was installed in anticipation of an inward shift in air flow. As shown in figure 17, at 1500 pounds per square foot the effect of these changes was negligible. Because of time limitations, investigation of configuration D was discontinued without

obtaining performance at 620 pounds per square foot. It was believed that the higher pressure losses of configuration D would lower the thrust obtainable by more than might be gained by any improvements in combustion efficiency resulting from more favorable diffuser velocity profiles.

Performance of the best configuration, H, obtained during this phase of investigation is shown in figure 18. Configuration H was the same as the original production configuration A, except that the outer fuel ring was moved upstream and the fuel sprayed in an upstream direction, and the fuel holes in all rings were reduced from 0.041- to 0.027-inch diameter. Also, a fourth fuel ring was added in the place originally occupied by the outer ring, but it was never actually used for spraying fuel. However, it must be considered as an essential part of configuration H, inasmuch as burning did not occur on the outer flame-holder gutter at the two lowest pressure levels when this inoperative fuel ring was removed. The effect of the inoperative fuel ring was probably that of blocking or partly blocking the louvers in the outer flame-holder gutter. It will be noted that the performance at all except the lowest pressure level (620 lb/sq ft abs) was about the same as the original configuration. For pressures of 2750 and 1500 pounds per square foot, peak combustion efficiency was between 0.85 and 1.0 and occurred at afterburner fuel-air ratios between 0.030 and 0.040. Maximum combustion efficiency at 620 pounds per square foot absolute was about 0.54. The optimum fuel distribution to the inner, middle, and outer fuel rings was approximately 15, 55, and 30 percent, respectively.

A direct comparison of the combustion efficiencies obtained with the original configuration and configuration H is presented in figure 19 for operation at pressures of 1500 and 620 pounds per square foot absolute. The only significant improvement was obtained at the lower pressure level, where the efficiency was improved about 0.17 at a fuel-air ratio of 0.05. A comparison of the data of figures 11 and 18 shows that, whereas the maximum exhaust-gas temperature at a pressure of 620 pounds per square foot was only 2380° R for the original configuration because of the low combustion efficiency, the maximum exhaust-gas temperature of configuration H was about 2950° R. This increase in temperature gave an increase in maximum thrust from 1500 to 1660 pounds and a reduction in specific fuel consumption at stoichiometric fuel-air ratio (0.067) from 3.70 to 3.15 pounds of fuel per hour per pound of net thrust. Further efforts to improve the performance of the afterburner, without configuration changes of such magnitude that production might be disturbed, did not appear fruitful.

#### Operational Characteristics

One of the operation difficulties exhibited by the configurations incorporating the anti-screech bars between the flame-holder gutters (flame holder A) was the lack of flame propagation between these two

gutters. The trend shown in figure 20 is a result of this lack of cross-propagation. These data for configuration F show higher combustion efficiency at a pressure level of 1500 than at 2600 pounds per square foot. Observations of the combustion through a periscope revealed that, whereas both gutters were holding flame at the 2750 and 1500 pound pressure levels, only the inner gutter held flame at a pressure level of 2600 pounds per square foot. Apparently the ignition flame streak from the "hot-shot" pilot did not ignite the fuel near the outer gutter on this particular start, and the flame failed to propagate to the outer gutter, resulting in a lower level of efficiency over the entire range of fuel-air ratios.

The operable ranges of the configurations discussed herein are defined by the bar charts of figure 21. The various factors limiting the operable ranges were (1) combustion instability described as rumble, buzz, or screech, depending on the frequency of the associated pressure pulsations (see ref. 3 for a discussion of these types of instability); (2) lean combustion blow-out; (3) rich combustion blow-out; (4) maximum area of the exhaust nozzle; and (5) maximum fuel flow obtainable. This latter limit is of course not a burner limitation. All these limits are denoted either by symbols or by shaded areas on the bar charts.

A brief résumé of the characteristics of the individual configurations is given in the following paragraphs:

Configuration A. - The original configuration operated without combustion instability over a range of fuel-air ratios from the lean blow-out limit, which varied from a fuel-air ratio of 0.004 at a pressure level of 2750 pounds per square foot to 0.017 at 620 pounds per square foot, to the value required to drive the exhaust nozzle wide open or to the fuel-air ratio at which rich blow-out occurred. The fuel-air ratio for rich blow-out varied considerably with changes in the fuel distribution to the three manifold rings (fig. 21(c)); the minimum value for rich blow-out was 0.054.

Configuration B. - At pressure levels of 2600 and 1500 pounds per square foot, the maximum operable fuel-air ratio was limited by rumble. At 620 pounds per square foot, the maximum operable fuel-air ratio was limited by rich blow-out. Here again the maximum fuel-air ratio at rich blow-out varied markedly, as would be expected, with changes in fuel distribution to the three manifold rings, varying from 0.032 to 0.080. The lean blow-out limit at 620 pounds per square foot was not altered appreciably by covering the louvers in the flame holder.

Configuration C. - In comparing configuration C to configuration A, replacement of the outer group of flame stabilizing bars with radial V-gutters resulted in screeching combustion at fuel-air ratios above about 0.034 for operation at a pressure level of 2600 pounds per square foot. At 2750 pounds per square foot, the lean blow-out limit was identical to that of configuration A; but at 1500 pounds per square foot, the lean blow-out occurred at a slightly higher value of fuel-air ratio.

Configuration D. - Addition of the annular cascade assembly in the diffuser and replacement of the three-ring fuel manifold with a five-ring fuel manifold (configurations A and D) resulted in lean blow-out occurring at higher fuel-air ratios for operation at a pressure level of 1500 pounds per square foot. At this pressure level, the maximum fuel-air ratio for configuration D was limited by the exhaust nozzle reaching maximum area. The occurrence of this limitation for configuration D and not for configuration A was due to the higher pressure loss through the afterburner for configuration D, since, as shown earlier, the efficiencies for configurations A and D were about equal.

Configuration E. - Changing the direction of fuel spray of the inner and outer rings from downstream to upstream (configurations A and E) caused the maximum operable fuel-air ratio to be limited severely by screech at pressure levels of 2750 and 2600 pounds per square foot and by rumble at the lower pressures. The change from downstream to upstream injection would tend to aggravate the conditions of homogeneous charge which are believed to produce screeching combustion. However, inasmuch as later configurations sprayed fuel in the upstream direction from the outer fuel manifold without encountering screech, the conditions producing screech in configuration E were evidently concerned with only the inner flame-holder ring. Configuration E was the only configuration spraying fuel upstream from the inner fuel ring and the only configuration encountering screech, with the exception of configuration C (anti-screech bars removed).

Configuration F. - With configuration F, which was the same as configuration A except that the outer fuel ring was moved  $8\frac{1}{4}$  inches upstream, no audible screech occurred at high pressure levels. At 1500 pounds per square foot, however, rough combustion occurred at fuel-air ratios above 0.0445. This increase of mixing length between the point of fuel injection and the outer gutter thus increased the tendency for heat-driven types of instability. A comparison of configurations E and F, however, shows that the inner gutter may be more prone to screech than the outer gutter. Operation was not possible at 620 pounds per square foot, possibly as a result of misalignment of the fuel with respect to the outer gutter.

Configuration G. - The effect of altering the fuel stratification near the outer gutter by nonaxial components of the fuel jets (configurations F and G) is seen to be a slight reduction in the maximum operable fuel-air ratio at a pressure level of 1500 pounds per square foot. Configuration G was limited by screech, whereas configuration F was limited by a combination of rumble and buzz. Here again steady operation was not possible at 620 pounds per square foot; however, operation was possible at lower pressures (not shown) than for configuration F.

Configuration H. - Configuration H, which was identical to configuration G except that the fuel pressures were increased, gave suitable characteristics at all pressure levels, except on one occasion where for a particular fuel distribution screech occurred at a fuel-air ratio of 0.041 at a pressure level of 1500 pounds per square foot. Much of the improvement in operational range at low pressure level (i.e., ability to operate at 620 lb/sq ft abs) is probably due to better circumferential fuel distribution produced by the increase in fuel pressure.

Configuration I. - Configuration I was similar to H except for a small change in the angularity of the fuel holes in the outer fuel manifold. As might be expected with a more stratified fuel-air pattern near the outer gutter, the lean blow-out limits occurred at lower fuel-air ratio with configuration I.

#### CONCLUDING REMARKS

During the investigation reported herein, the performance of the J40-WE-8 afterburner was evaluated at burner-inlet pressures as low as 620 pounds per square foot, a value somewhat below the minimum pressure in the engine specification (730 lb/sq ft). Numerous modifications were made to the flame holder, fuel-injection system, and diffuser in an effort to improve the performance at the lowest pressure level without greatly altering the mechanical design of the burner components, in order to avoid production delay. As a result several changes which were indicated to be desirable as a result of previous investigations were not made in the phase of the program reported herein. The best configuration resulting from this investigation differed from the original configuration only in details of the fuel system. Inasmuch as peak combustion efficiency of the original configuration was high at pressures at or above 1500 pounds per square foot, no appreciable improvement was possible; however, at the lowest pressure level of 620 pounds per square foot the peak efficiency was raised from 0.47 to 0.54, and over most of the comparable range of fuel-air ratios, the efficiency was increased about 0.17. This resulted in an increase in the maximum exhaust-gas temperature from 2380° to 2950° R; an increase in maximum net thrust from 1500 to 1660 pounds; and a reduction in specific fuel consumption at stoichiometric fuel-air ratio (0.067) from 3.70 to 3.15 pounds of fuel per hour per pound of net thrust. The configuration giving the best performance, however, was subject to buzzing combustion under certain operating conditions.

Lewis Flight Propulsion Laboratory  
National Advisory Committee for Aeronautics  
Cleveland, Ohio

## APPENDIX - SYMBOLS AND METHODS OF CALCULATION

## Symbols

The following symbols are used in this report:

A	cross-sectional area, sq ft
B	thrust-scale reading, lb
$C_v$	velocity coefficient, ratio of scale jet thrust to rake jet thrust
D	external drag of installation, lb
$D_r$	drag of exhaust-nozzle survey rake, lb
$F_j$	jet thrust, lb
$F_n$	net thrust, lb
f/a	fuel-air ratio
g	acceleration due to gravity, 32.2 ft/sec <sup>2</sup>
H	total enthalpy of air, Btu/lb
P	total pressure, lb/sq ft abs
p	static pressure, lb/sq ft abs
R	gas constant, 53.4 ft-lb/(lb)(°R)
T	total temperature, °R
t	static temperature, °R
V	velocity, ft/sec
$W_a$	air flow, lb/sec
$W_f$	fuel flow, lb/hr
$\frac{W_{f,t}}{F_{n,s}}$	specific fuel consumption based on total fuel flow and scale net thrust, lb/(hr)(lb thrust)
$W_g$	gas flow, lb/sec
$\gamma$	ratio of specific heats for gases

$\eta$  combustion efficiency

$\lambda$  total enthalpy of fuel, Btu/lb

Subscripts:

a air

b afterburner

e engine

f fuel

i indicated

j jet

n exhaust-nozzle exit

s scale

t total

x inlet duct at frictionless slip joint

0 free-stream conditions

1 engine-inlet duct

5 turbine inlet

5' first-stage turbine-nozzle throat

6 afterburner inlet (turbine outlet)

7 flame-holder inlet

9 exhaust nozzle,  $4\frac{1}{8}$  inches upstream of exhaust-nozzle outlet

9' exhaust nozzle (with standard engine tail pipe)

#### Methods of Calculation

Temperatures. - Static temperatures were determined from thermocouple-indicated temperatures with the following relation:

$$t = \frac{T_i}{1 + 0.85 \left[ \left( \frac{P}{P_1} \right)^{\frac{\gamma-1}{\gamma}} - 1 \right]} \quad (1)$$

where 0.85 is the impact recovery factor for the type of thermocouple used. Total temperatures were determined by the adiabatic relation between temperatures and pressures.

Airspeed. - The equivalent airspeed was calculated from the ram-pressure ratio by the following equation, with complete pressure recovery at the engine-inlet assumed:

$$V_0 = \sqrt{\frac{2\gamma_1 g R T_1}{\gamma_1 - 1} \left[ 1 - \left( \frac{P_0}{P_1} \right)^{\frac{\gamma_1 - 1}{\gamma_1}} \right]} \quad (2)$$

Air flow and gas flow. - Because of erratic measurements at the engine inlet during the afterburning program, the air flow was determined from measurements at the turbine inlet (station 5). Inasmuch as the turbine nozzles were choked for the range of conditions investigated, the gas flow at the turbine-nozzle throat could be determined from the following equation:

$$W_{g,5'} = \frac{P_5 A_{5'}}{\sqrt{T_5}} \sqrt{\frac{g}{R}} \frac{\sqrt{\gamma_5}}{\left( \frac{\gamma_5 + 1}{2} \right)^{\frac{\gamma_5 + 1}{2(\gamma_5 - 1)}}} \quad (3)$$

The effective turbine-nozzle throat area  $A_{5'}$  was determined from previous tests for the same range of engine operating conditions investigated herein when the engine inlet-air flow calculations were reliable. The air flow or gas flow at any station throughout the engine and afterburner could then be obtained from  $W_{g,5'}$  by adding or subtracting the various factors of engine fuel flow, afterburner fuel flow, and compressor bleed air.

Afterburner fuel-air ratio. - The afterburner fuel-air ratio is defined as the ratio of the weight flow of fuel injected in the afterburner to the weight flow of unburned air entering the afterburner from the engine. Weight flow of unburned air was determined by assuming that

the fuel injected in the engine was completely burned. This assumption of 100 percent combustion efficiency in the engine results in only a small error in afterburner fuel-air ratio, because the engine was operated where combustion efficiency  $\eta_e$  is known to be high. Afterburner fuel-air ratio was calculated from the equation

$$(f/a)_b = \frac{W_{f,b}}{3600 W_{a,6} - \frac{W_{f,e}}{0.067}} \quad (4)$$

where 0.067 is the stoichiometric fuel-air ratio for the engine fuel.

Exhaust-gas total temperature. - The total temperature of the exhaust gas was calculated from the exhaust-nozzle-outlet total pressure, scale jet thrust, velocity coefficient, and gas flow by means of the following equation:

$$T_j = \left( \frac{F_{j,s}}{C_v} \right)^2 \left( \frac{g}{2R} \right) \left( \frac{\gamma_9 - 1}{\gamma_9} \right) \frac{1}{W_{g,9}^2 \left[ 1 - \left( \frac{P_0}{P_9} \right)^{\frac{\gamma_9 - 1}{\gamma_9}} \right]} \quad (5)$$

The velocity coefficient  $C_v$ , which is defined as the ratio of scale jet thrust to rake jet thrust, was determined to be 0.98 from nonafterburning data over a wide range of exhaust-nozzle pressure ratios.

Combustion efficiency. - Afterburner combustion efficiency was obtained by dividing the enthalpy rise through the afterburner by the heat content of the afterburner fuel and unburned engine fuel as shown in the following equation:

$$\eta_b = \frac{3600 W_{a,6} (H_{a,9} - H_{a,6}) + W_{f,e} (\lambda_{e,9} - \lambda_{e,6}) + W_{f,b} \lambda_{b,9}}{18,700 W_{f,b} + (1 - \eta_e) W_{f,e} 18,700} \quad (6)$$

where 18,700 (Btu/lb) is the lower heating value of the engine fuel and afterburner fuel. The enthalpies of the products of combustion were determined from temperature-enthalpy charts for air and from temperature-enthalpy charts for fuels having the same hydrogen-carbon ratios as the fuels used in this investigation (see ref. 3). The charts used for obtaining fuel enthalpies were based on a fuel-inlet temperature of 80° F. Dissociation was not considered in this analysis, because its effect is negligible for the range of exhaust-gas temperatures encountered in this investigation.

Augmented thrust. - The jet thrust of the installation was determined from the balance-scale measurements by the following equation:

$$F_{j,s} = B + D + D_r + \frac{W_{a,1} V_x}{g} + A_x(P_x - P_0) \quad (7)$$

The last two terms of this expression represent momentum and pressure forces on the installation. External drag of the installation was determined with the engine inoperative, and the drag of the water-cooled exhaust-nozzle survey rake was measured by an air-balance piston mechanism.

Scale net thrust was obtained by subtracting the equivalent free-stream momentum of the inlet air from the scale jet thrust:

$$F_{n,s} = F_{j,s} - \frac{W_{a,1} V_0}{g} \quad (8)$$

Standard engine thrust. - Standard engine thrust is defined as the engine thrust obtainable at rated speed with the standard engine tail pipe and with the same turbine-outlet pressures and temperatures that were encountered with afterburning. The standard engine thrust was calculated from the average measurements obtained at each flight condition during the afterburning program of total pressure and temperature at the turbine outlet, the engine gas flow (no compressor bleed air for afterburner cooling), and from the previously determined total-pressure loss across the standard tail pipe:

$$F_{j,9'} = C_v \left[ \frac{(W_{a,1} + \frac{W_{f,e}}{3600})}{g} \right] \sqrt{\frac{2\gamma_6 g R T_6}{(\gamma_6 - 1)} \left[ 1 - \left( \frac{P_0}{0.97 P_6} \right)^{\frac{\gamma_6 - 1}{\gamma_6}} \right]} \quad (9)$$

Experimental data indicated that the total-pressure loss across the standard tail pipe was approximately  $0.03 P_6$  at rated engine speed. The exhaust-nozzle total pressure  $P_{9'}$  is therefore equal to  $0.97 P_6$ . The velocity coefficient  $C_v$  was determined to be 0.97 from calibration of the engine with the standard engine tail pipe and exhaust nozzle.

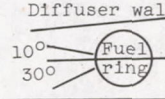
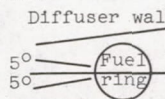
Standard engine net thrust was obtained by subtracting the equivalent free-stream momentum of the inlet air from the standard engine jet-thrust:

$$F_{n,9'} = F_{j,9'} - \frac{W_{a,1} V_0}{g} \quad (10)$$

## REFERENCES

1. Bragdon, Thomas A., Lewis, George D., and King, Charles H.: Interim Report on Experimental Investigation of High Frequency Oscillations in Ramjet Combustion Chambers. M.I.T. Meteor Rep. UAC-53, Res. Dept., United Aircraft Corp., Oct. 1951. (BuOrd Contract NOrd 9845.)
2. Conrad, E. William., and Campbell, Carl E.: Altitude Wind Tunnel Investigation of High-Temperature Afterburners. NACA RM E51L07, 1952.
3. Turner, L. Richard, and Lord, Albert M.: Thermodynamic Charts for the Computation of Combustion and Mixture Temperatures at Constant Pressure. NACA TN 1086, 1946.

TABLE I. - COMPONENT COMBINATIONS AND FUEL-SPRAY DATA

Config-uration	Dif-fuser	Flame holder	Fuel system			Remarks
			Hole diam., in.	Location	Direction injected, upstream  downstream  (a)	
A	A	A	0.041	1/2 in. upstream of flame holder	Outer  · Middle  · Inner  ·	Original configuration
B	A	B	0.041	Same as configuration A	 ·  ·  ·	Flame holder B same as A except louvers capped
C	A	C	0.041	Same as configuration A	 ·  ·  ·	Flame holder A outer stringers removed; cross gutters added
D	B	A	0.041	Same as configuration A	 ·  ·  ·  ·  ·	Diffuser deflection unit added; 2-in. spacer added fore of diffuser
E	A	A	0.041	Same as configuration A	 ·  ·	Diffuser same as original, configuration A
F	A	A	0.041	Outer ring 8 1/4 in. upstream of other two rings	 ·  ·  ·	
G	A	A	0.041	Same as configuration F	 ·  ·  ·	Alternate holes in outer ring drilled as follows:  
H	A	A	0.027	Fourth ring (inactive) added where outer ring was removed in configuration F	 ·  ·  ·	All rings same as configuration G but smaller hole size
I	A	A	0.027	Same as configuration F	 ·  ·	Outer ring drilled as follows:  

(a) Symbols:

- < flame-holder gutter
- o fuel manifold



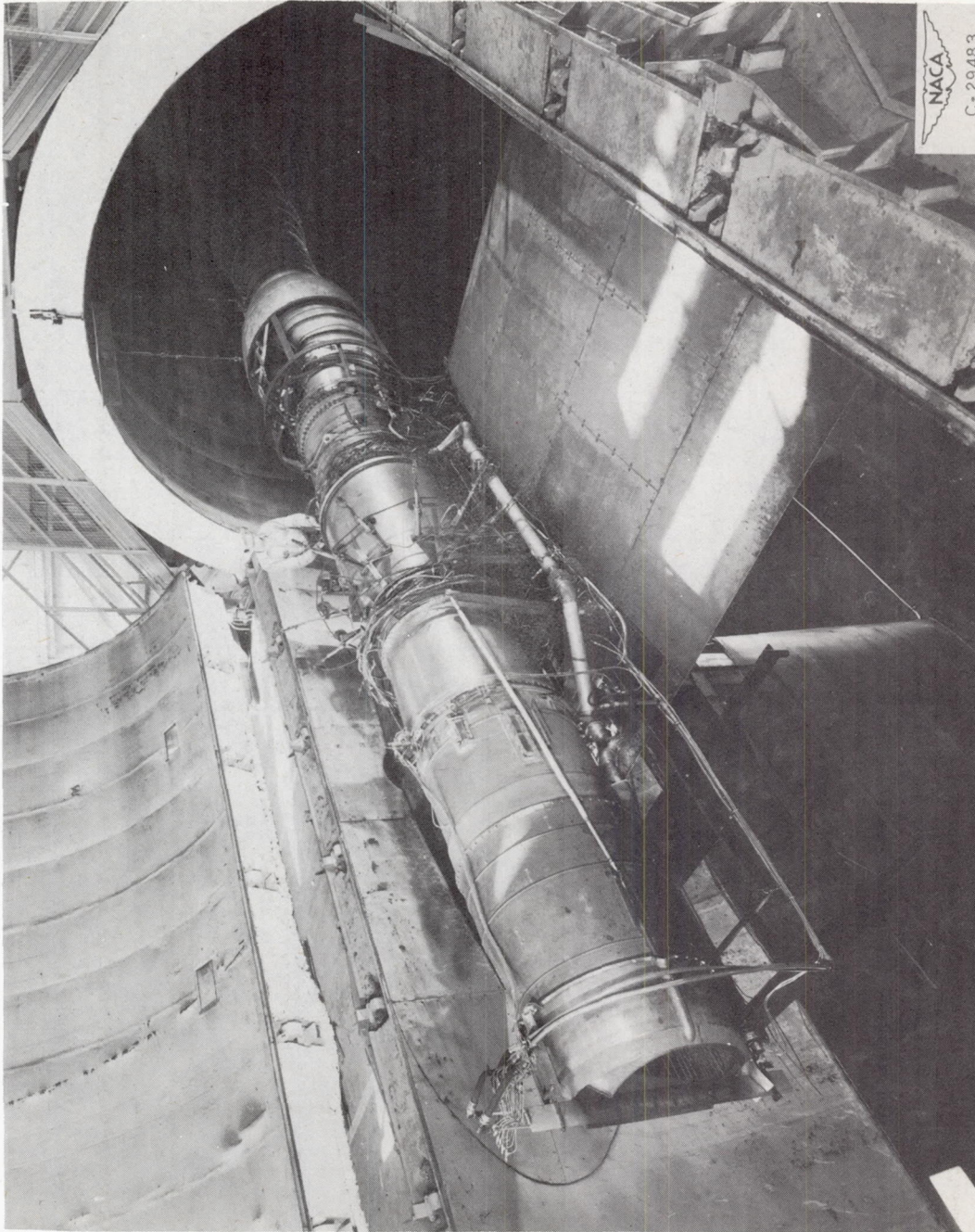
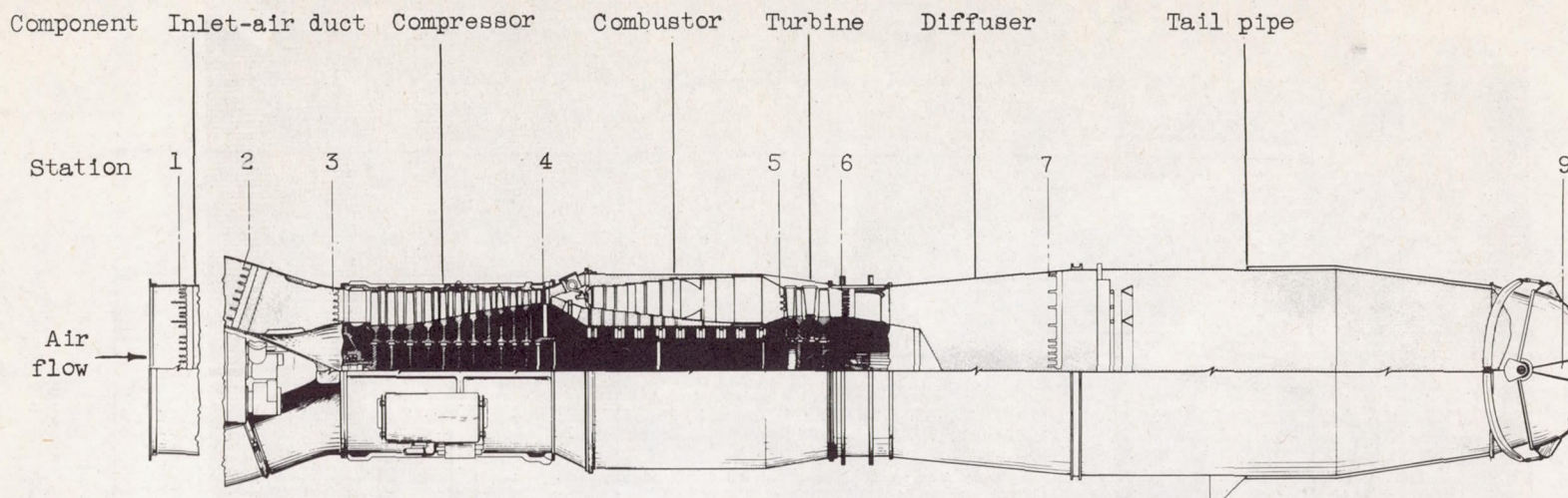


Figure 1. - Engine installed in altitude wind tunnel.



Station	Location	Total-pressure tubes	Static-pressure tubes	Wall static-pressure orifices	Thermocouples
1	Inlet-air duct	29	12	6	10
2	Engine inlet	18	0	4	0
3	Compressor inlet	23	3	7	0
4	Compressor outlet	18	0	3	6
5	Turbine inlet	5	0	0	<sup>a</sup> 10
6	Turbine outlet	20	0	8	24
7	Diffuser outlet	21	0	2	0
9	Exhaust-nozzle outlet	17	6	0	0

<sup>a</sup> Sonic probes



CD-2860

Figure 2. - Cross section of engine and afterburner showing stations at which instrumentation was installed.

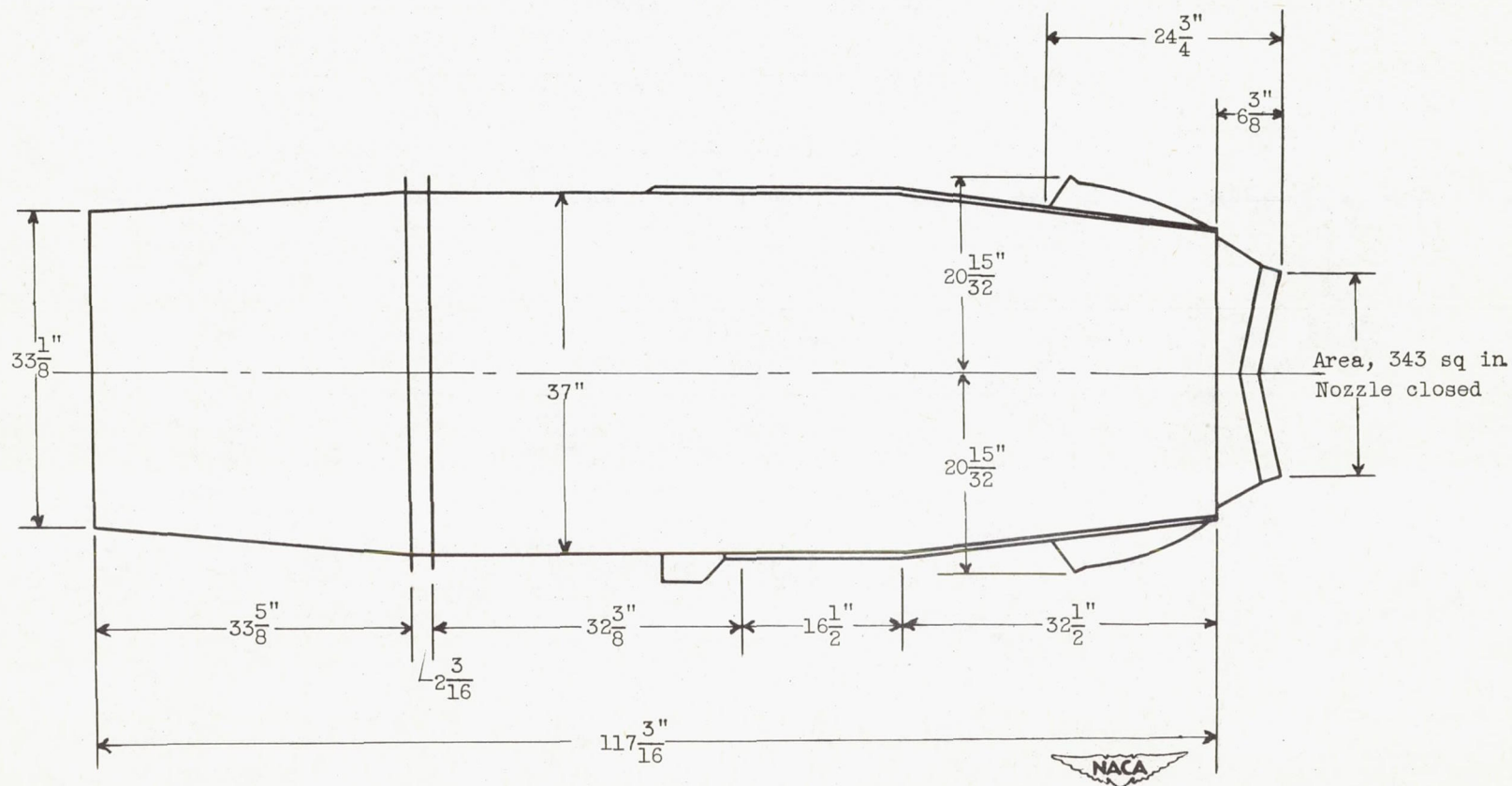
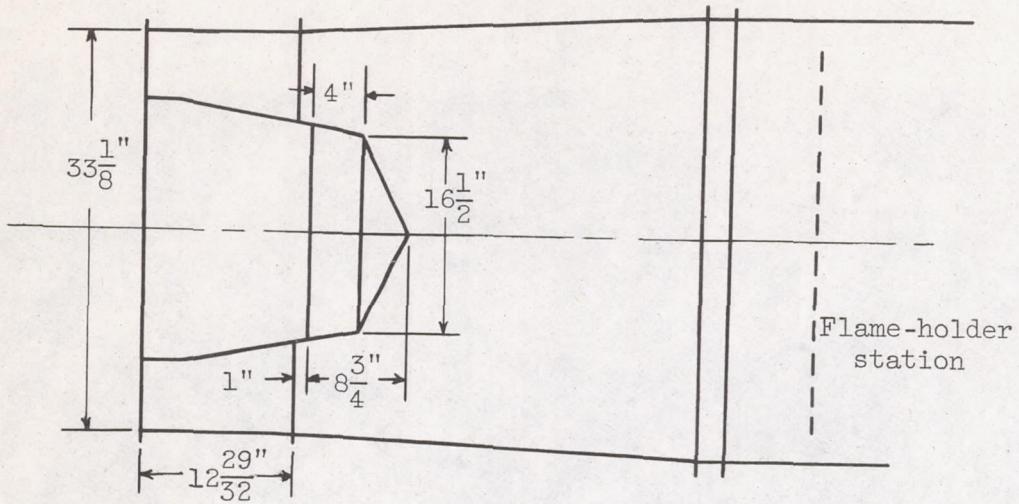
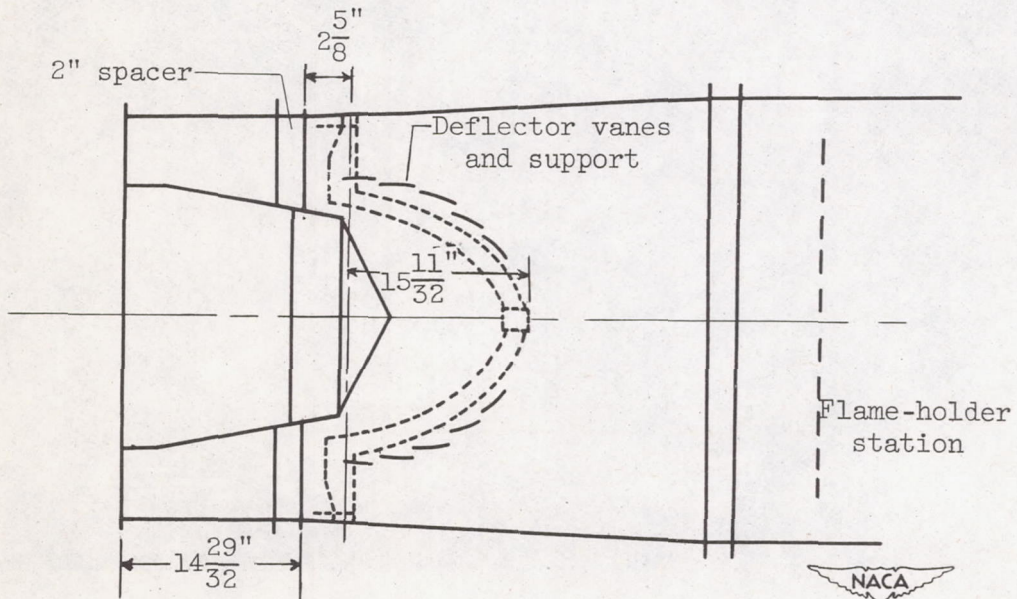


Figure 3. - Schematic drawing of afterburner shell and diffuser section.

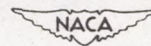


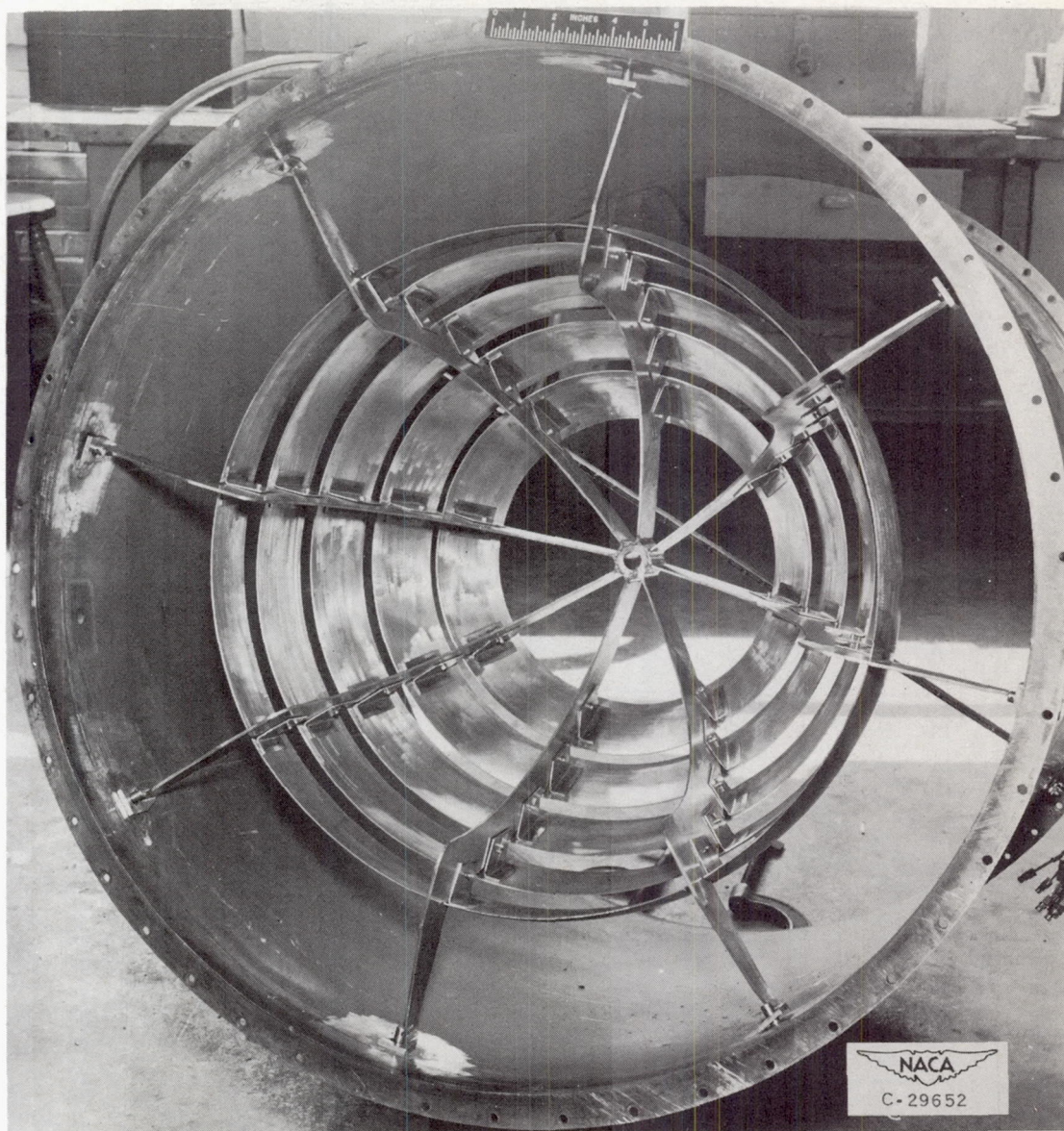
(a) Diffuser A, used with all configurations except configuration D.



(b) Diffuser B, used with configuration D.

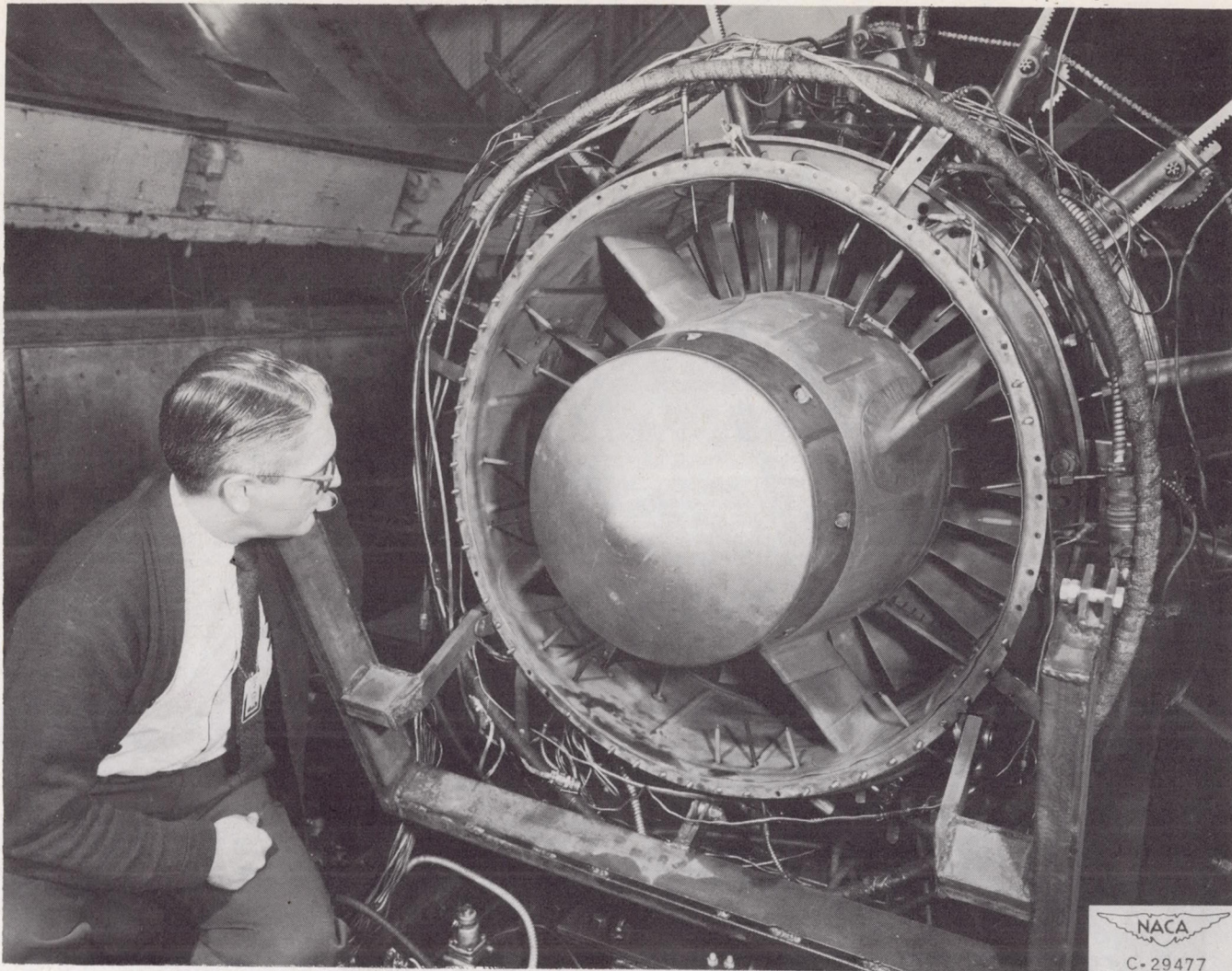
Figure 4. - Diffusers, vanes, and inner cone used in investigation.





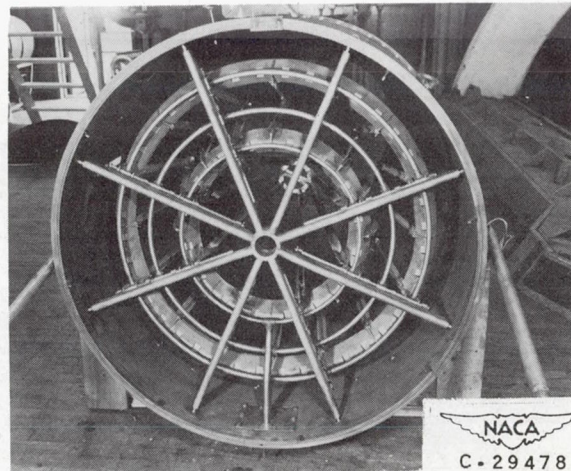
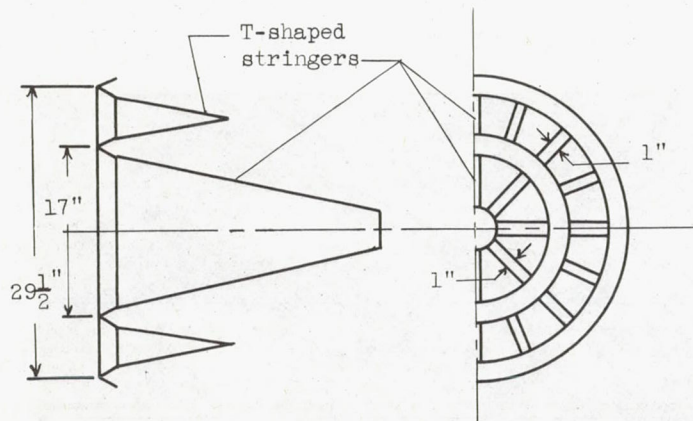
(c) Vanes used with configuration D.

Figure 4. - Continued. Diffusers, vanes, and inner cone used in investigation.

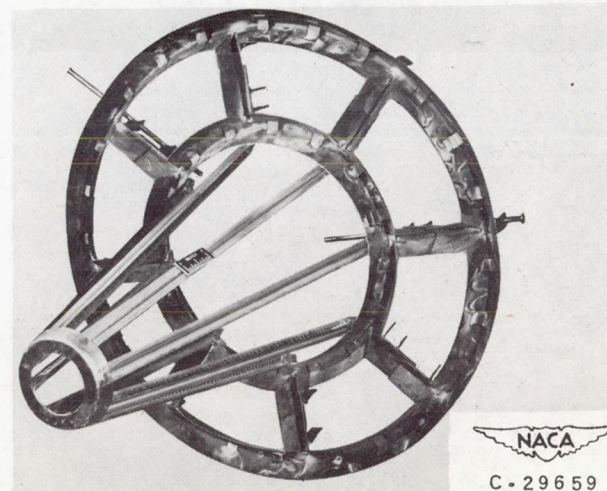
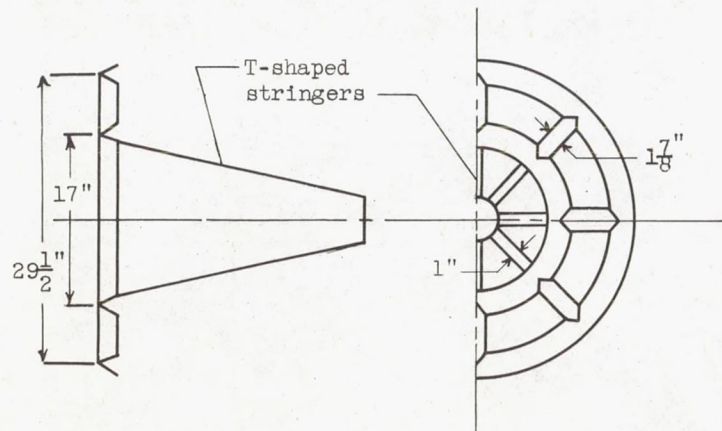


(d) Inner cone used with both diffusers.

Figure 4. - Concluded. Diffusers, vanes, and inner cone used in investigation.

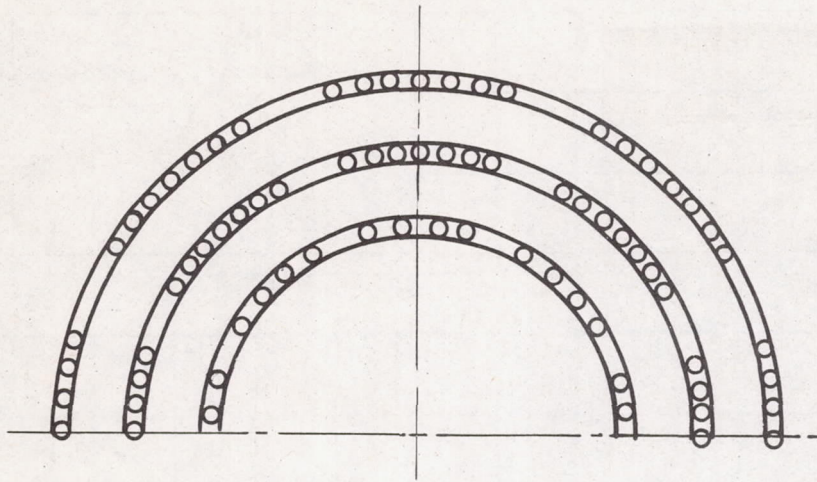


(a) Flame holder A, used with all configurations except configuration C (41.3 percent blockage).

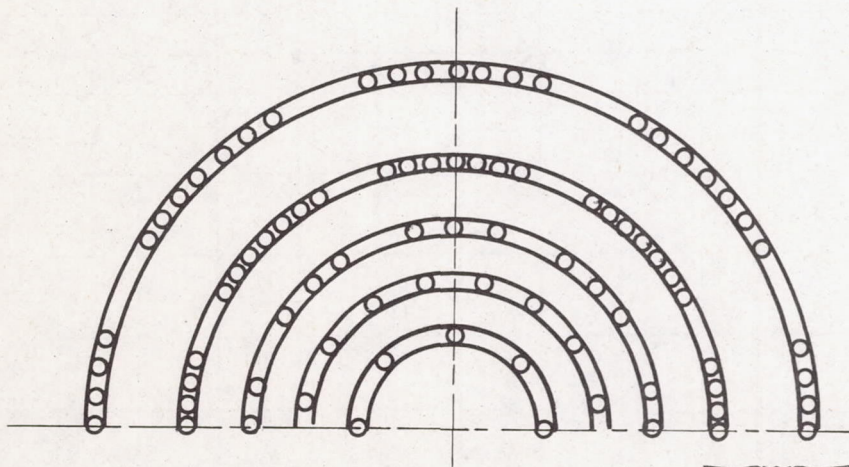


(b) Flame holder C, used with configuration C (38 percent blockage).

Figure 5. - Details of flame holders investigated.



(a) Three-ring fuel manifold.



(b) Five-ring fuel manifold.

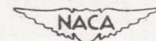
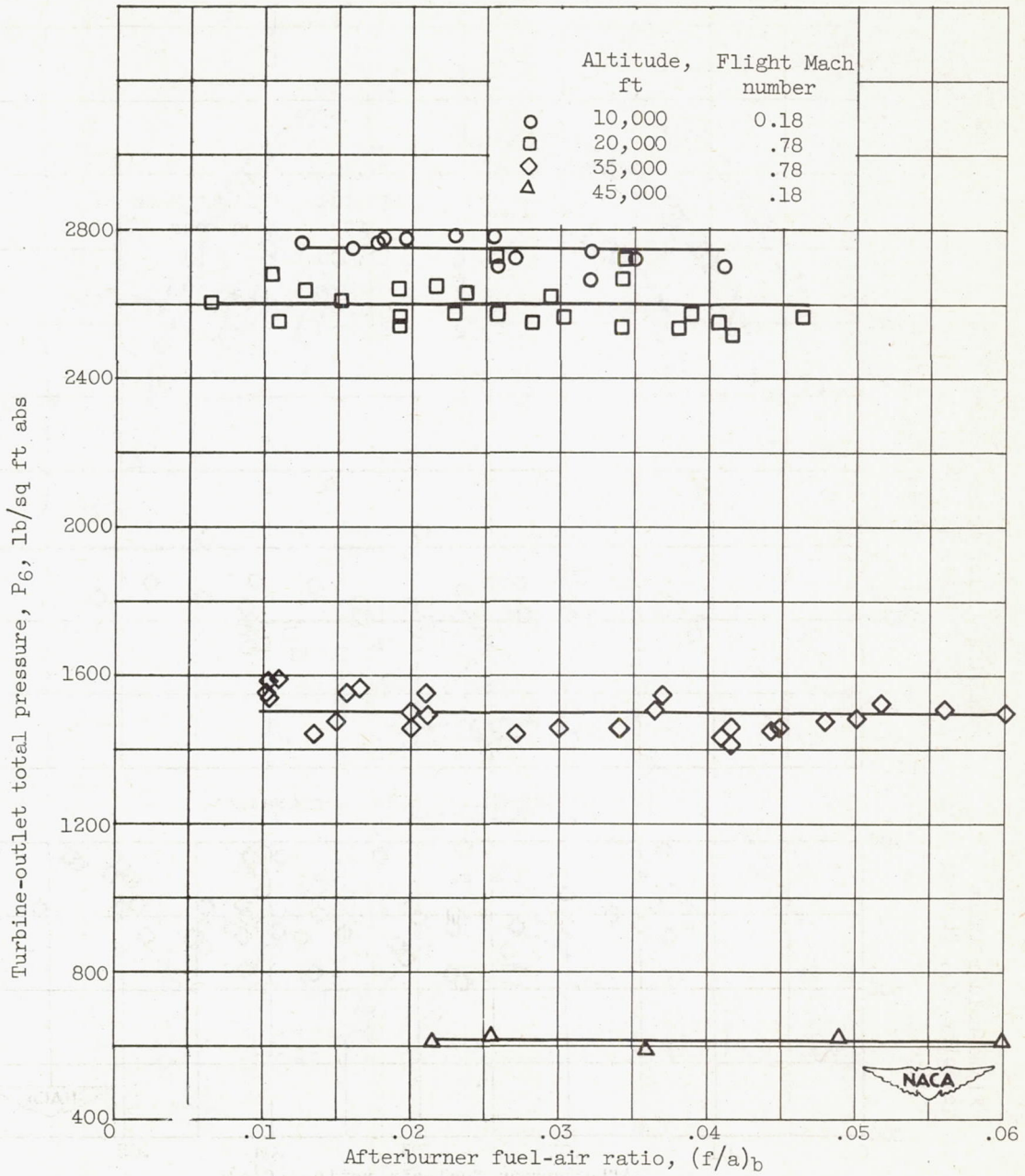
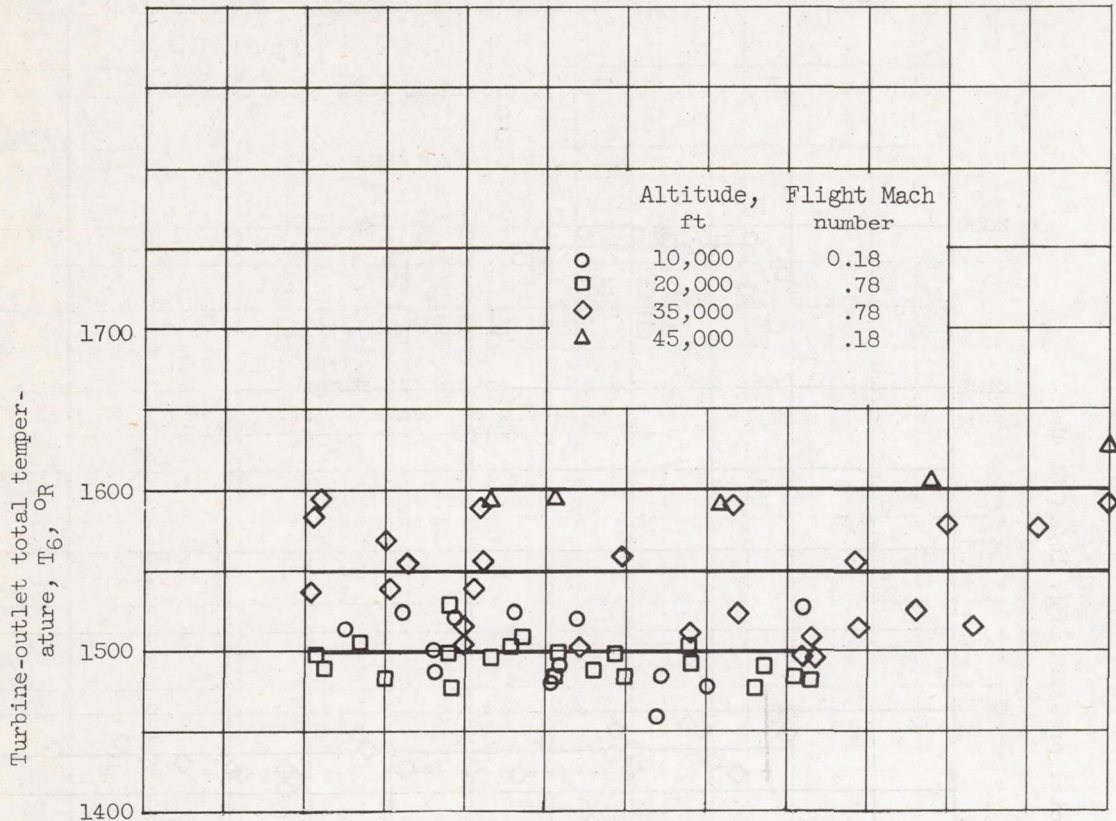


Figure 6. - Fuel manifolds used during investigation. Holes drilled only on one side of fuel rings.

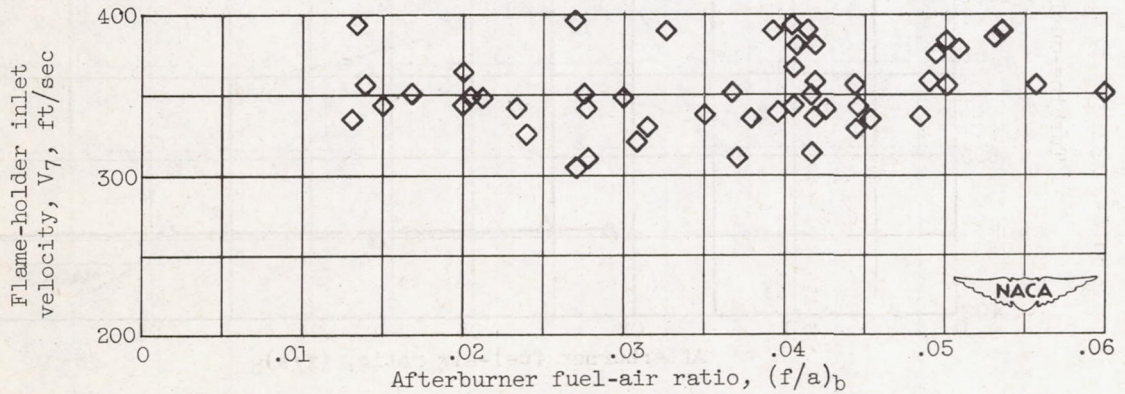


(a) Turbine-outlet total pressure.

Figure 7. - Flow conditions at combustion-chamber inlet.



(b) Turbine-outlet total temperature.



(c) Flame-holder inlet velocity.

Figure 7. - Concluded. Flow conditions at combustion-chamber inlet.

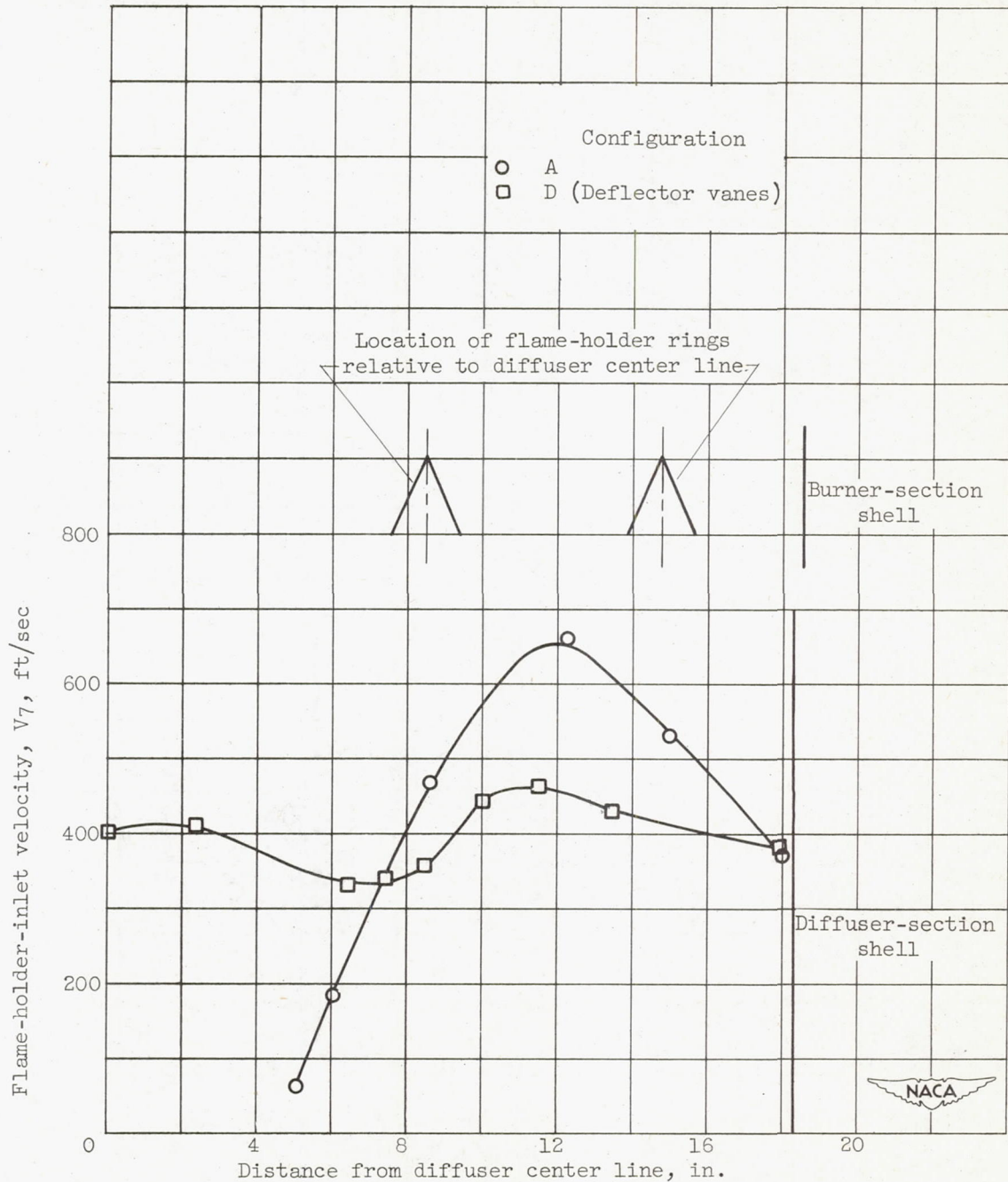
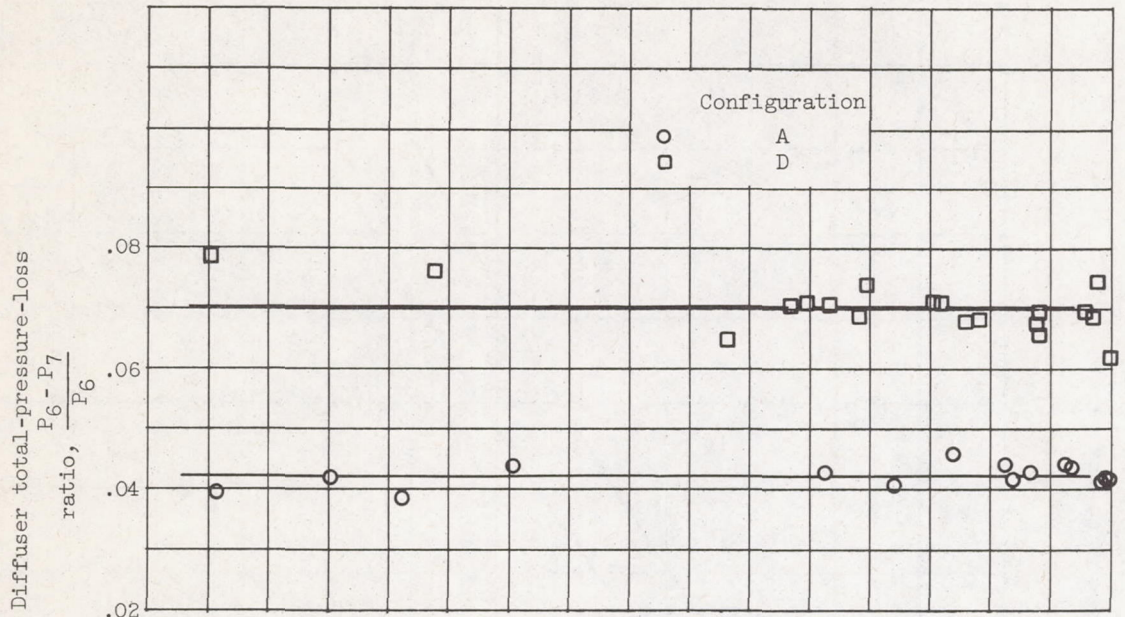
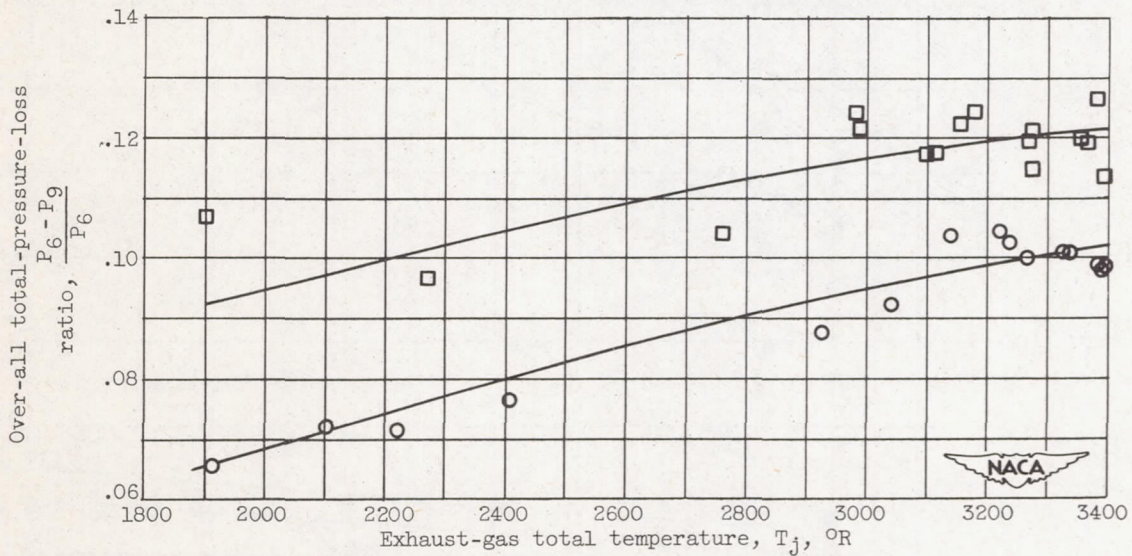


Figure 8. - Effect of diffuser deflector vanes on velocity profiles at flame-holder inlet. Burner-inlet pressure, 1500 pounds per square foot absolute.

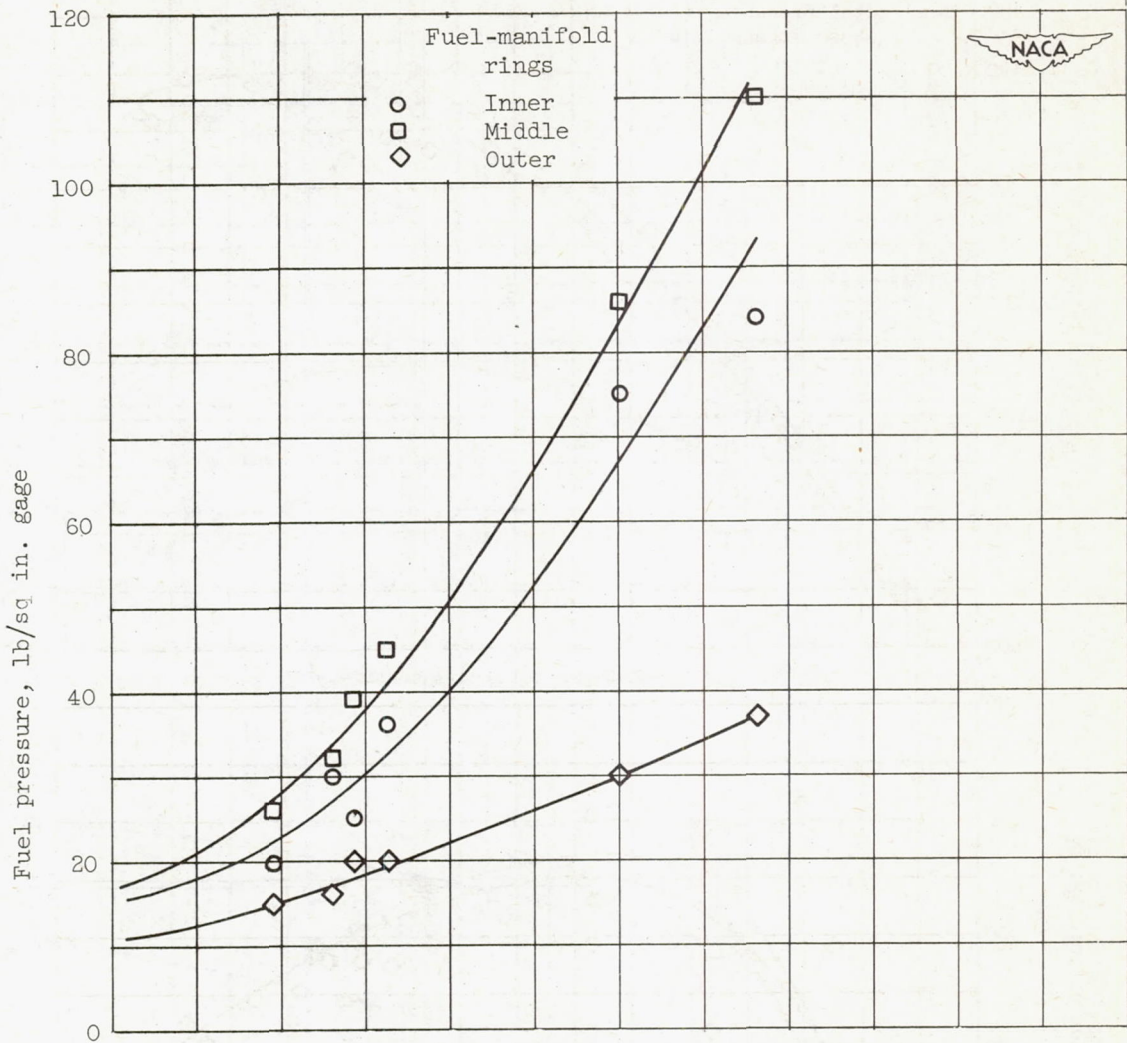


(a) Diffuser pressure-loss characteristics.

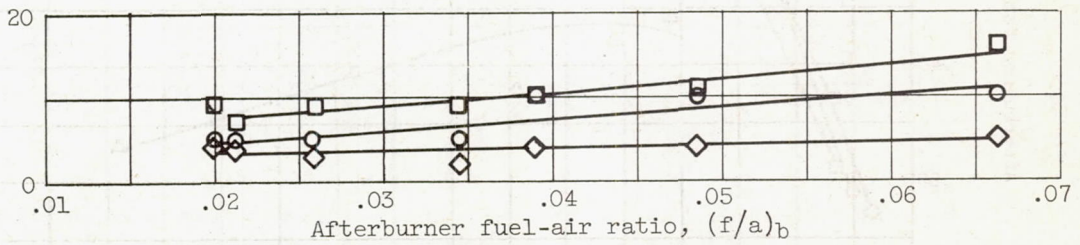


(b) Over-all pressure-loss characteristics.

Figure 9. - Effect of diffuser type on pressure-loss characteristics; burner-inlet pressure, 1500 pounds per square foot absolute.

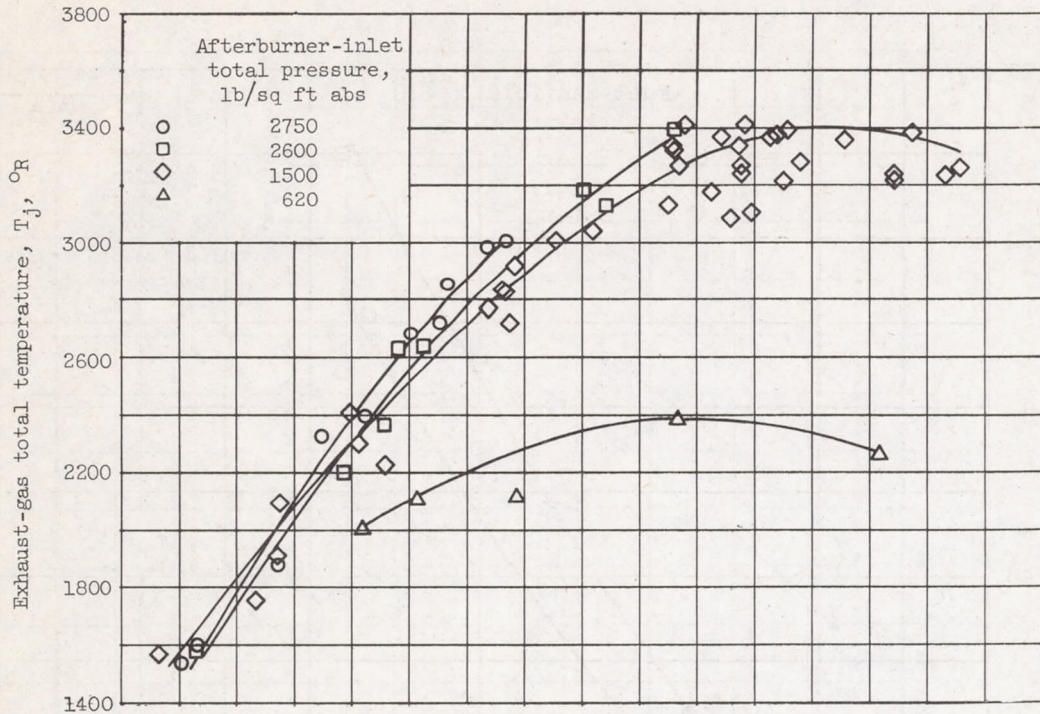


(a) Burner-inlet pressure, 2600 pounds per square foot absolute.

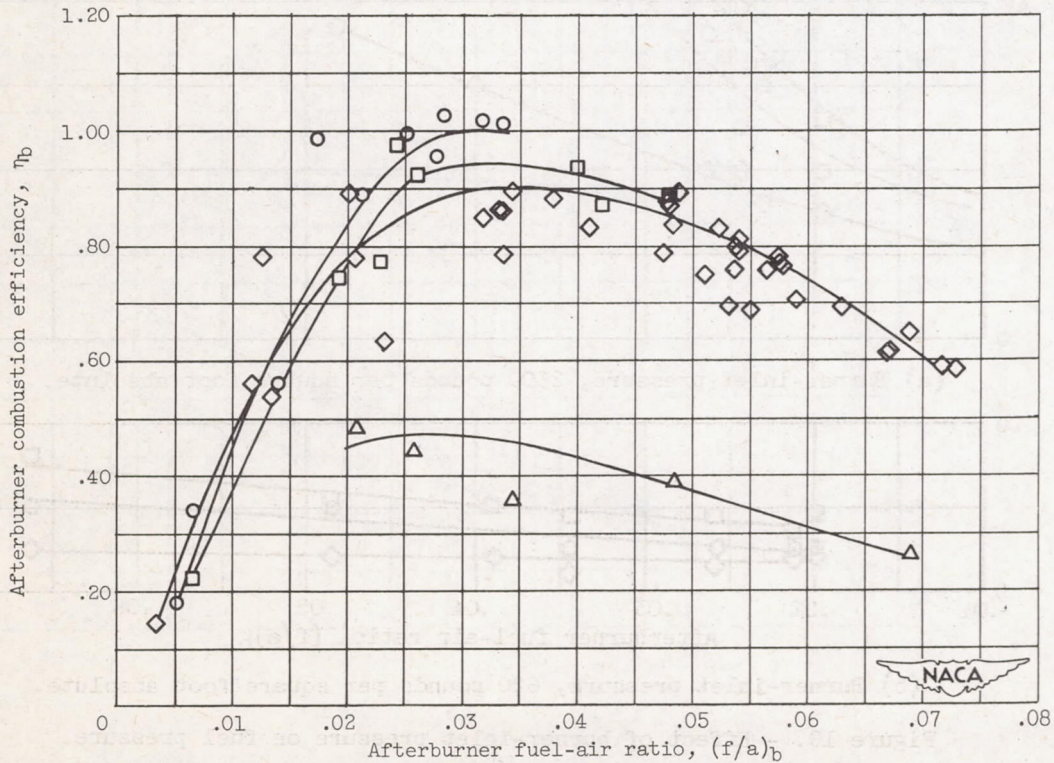


(b) Burner-inlet pressure, 620 pounds per square foot absolute.

Figure 10. - Effect of burner-inlet pressure on fuel pressure.

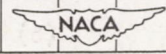


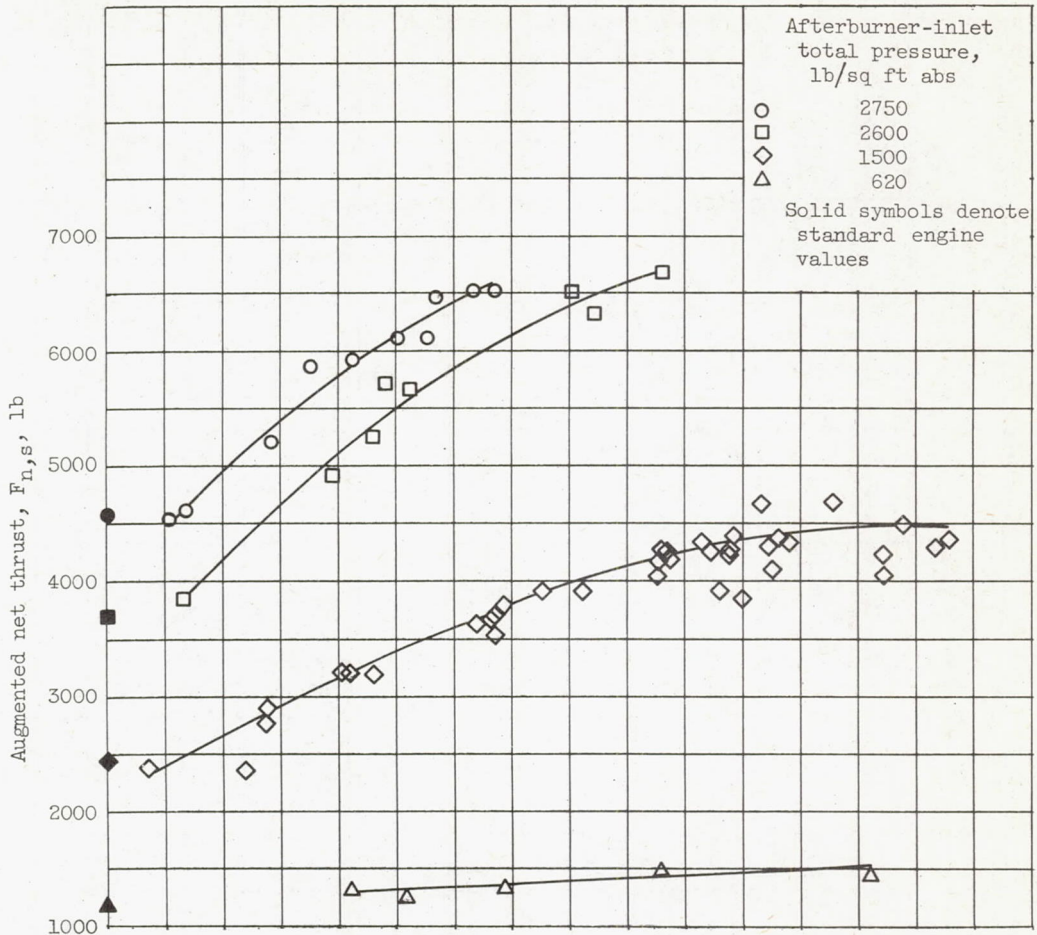
(a) Exhaust-gas total temperature.



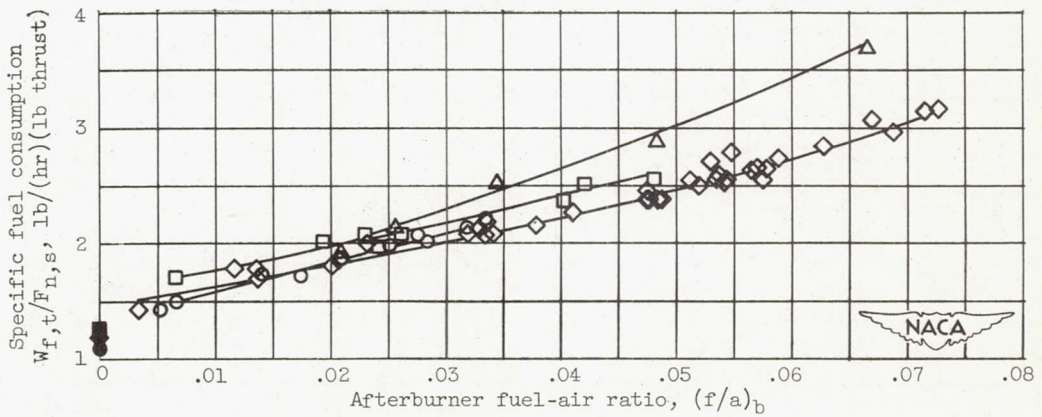
(b) Afterburner combustion efficiency.

Figure 11. - Performance of original configuration, A.





(c) Augmented net thrust.



(d) Specific fuel consumption.

Figure 11. - Concluded. Performance of original configuration, A.

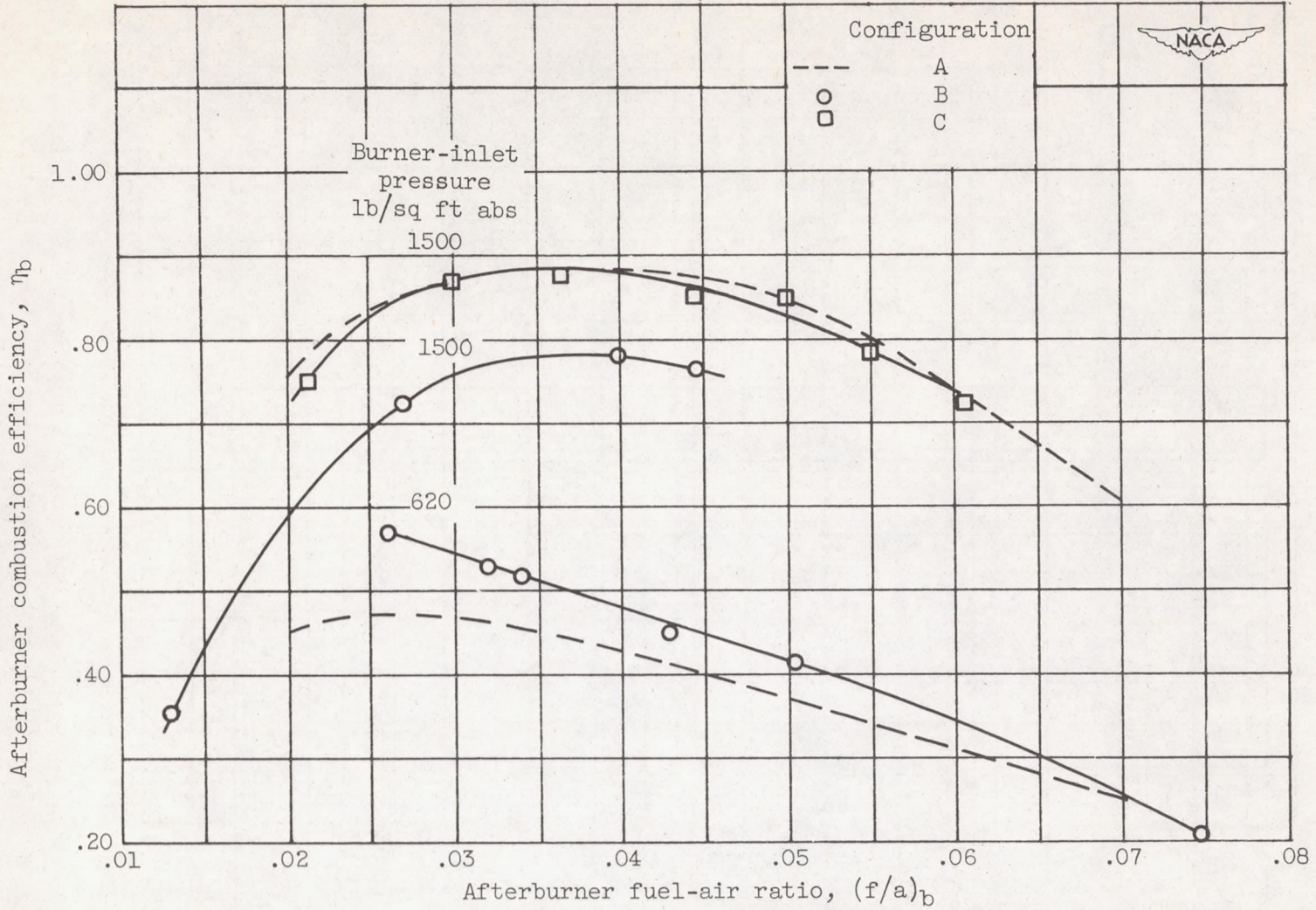


Figure 12. - Effect of flame-holder modifications on afterburner combustion efficiency.

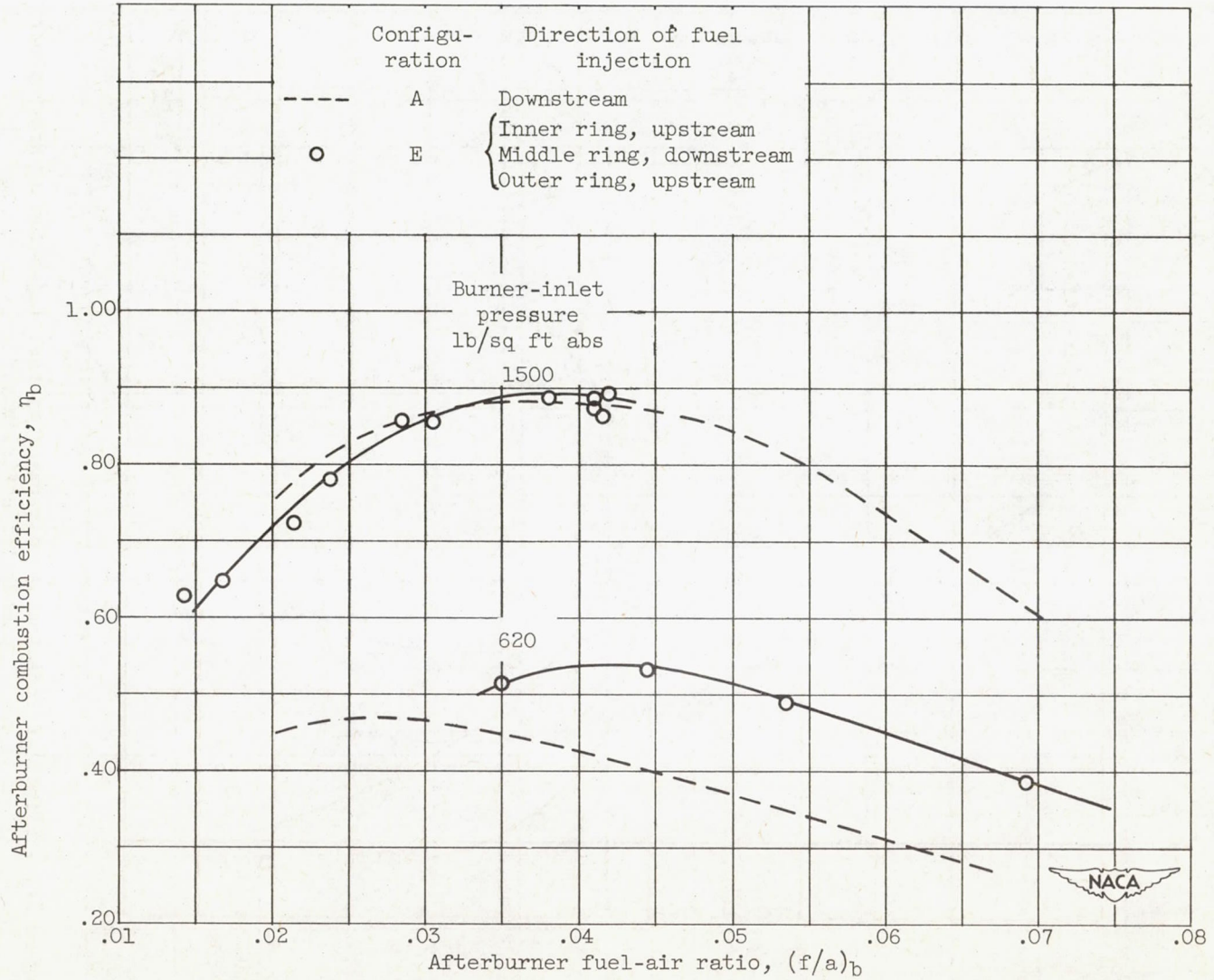


Figure 13. - Effect of fuel-spray direction on afterburner combustion efficiency.

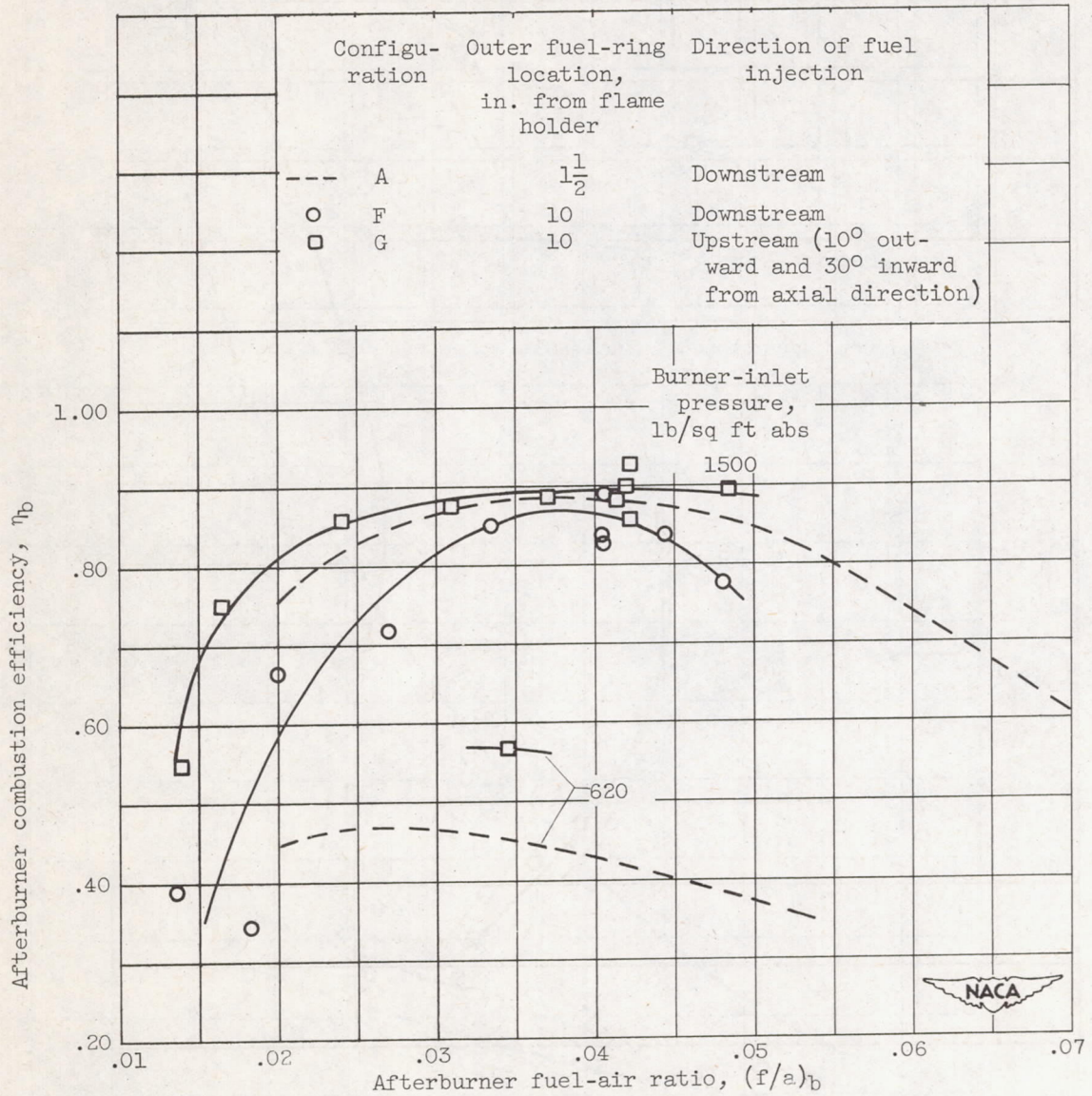
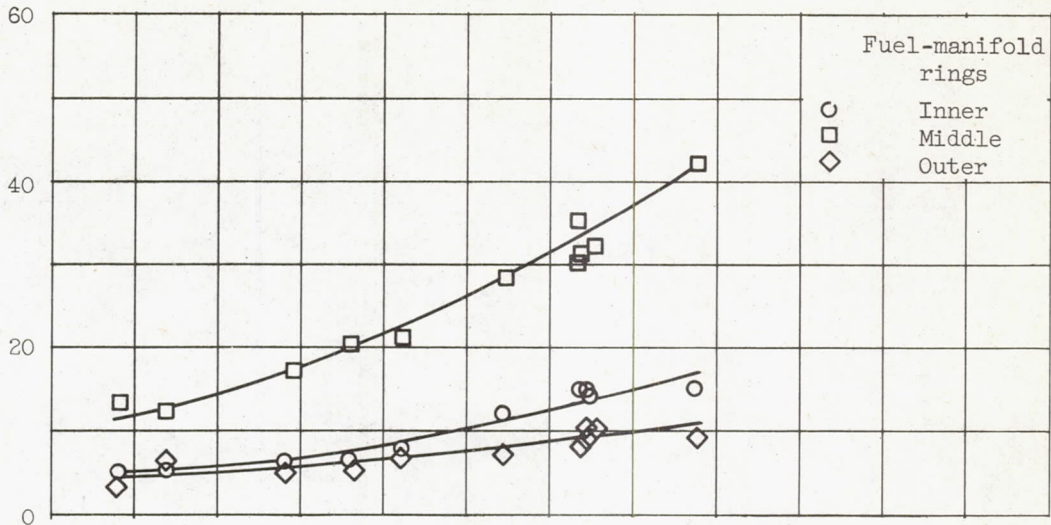
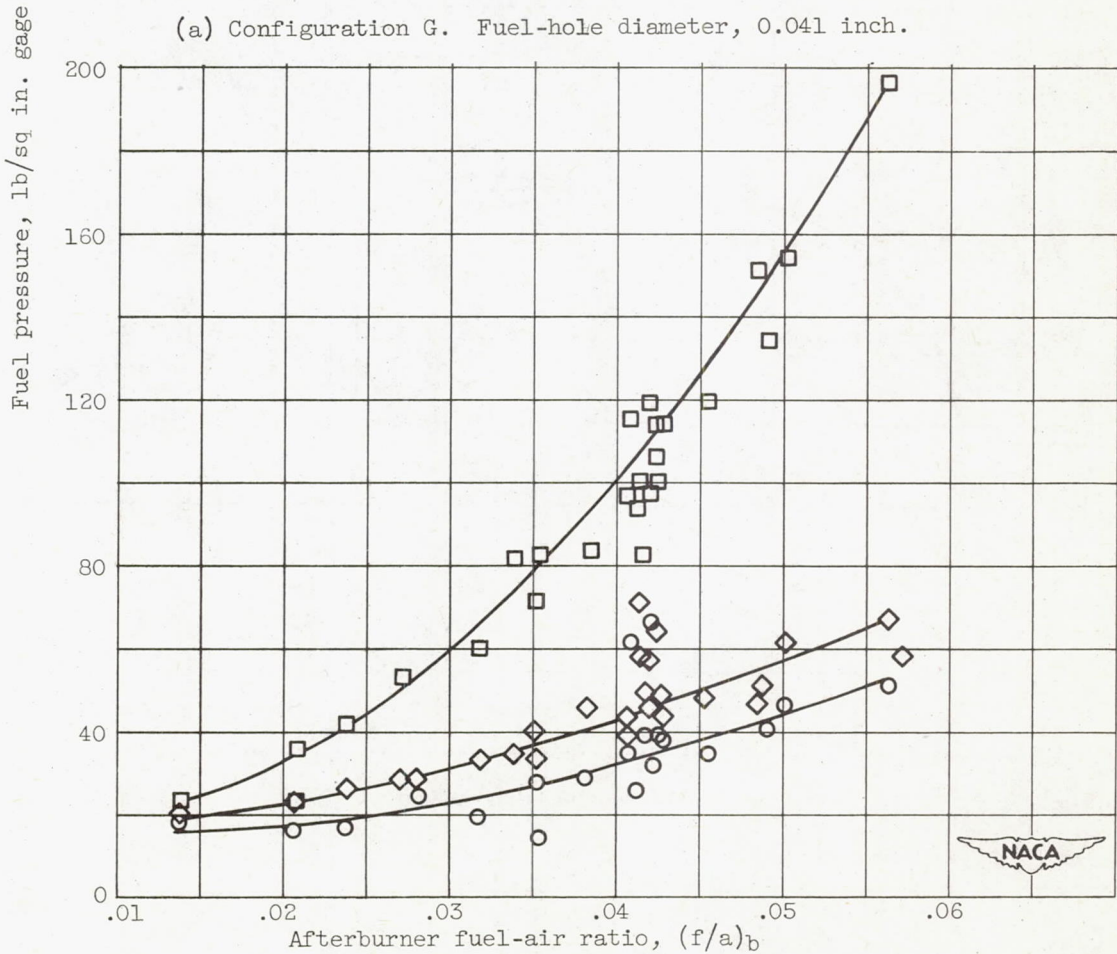


Figure 14. - Effect of location and direction of fuel injection on afterburner combustion efficiency.



(a) Configuration G. Fuel-hole diameter, 0.041 inch.



(b) Configuration H. Fuel-hole diameter, 0.027 inch.

Figure 15. - Comparison of fuel pressures for configurations G and H. Burner-inlet pressure, 1500 pounds per square foot absolute.



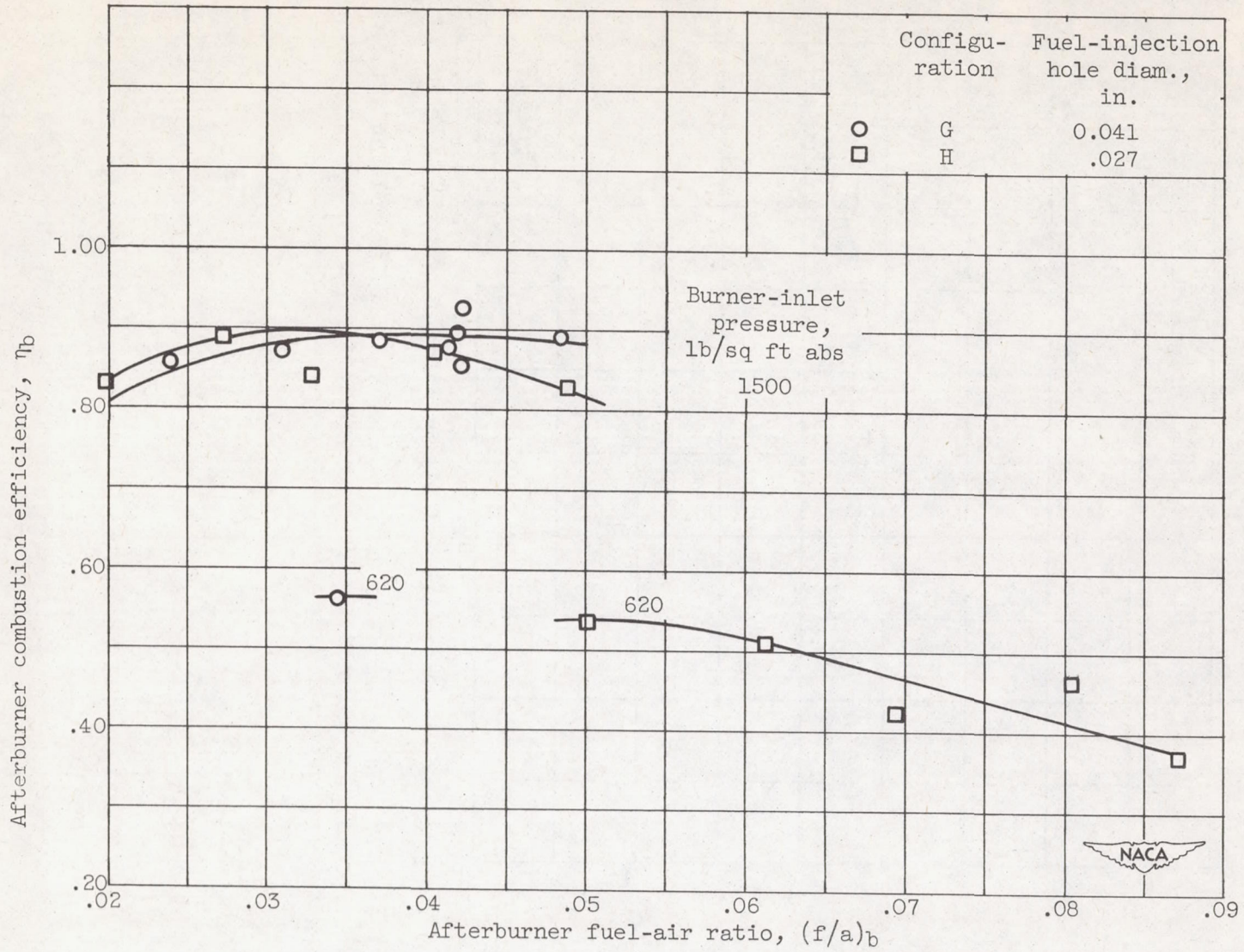


Figure 16. - Effect of fuel pressure (hole size) on afterburner combustion efficiency.

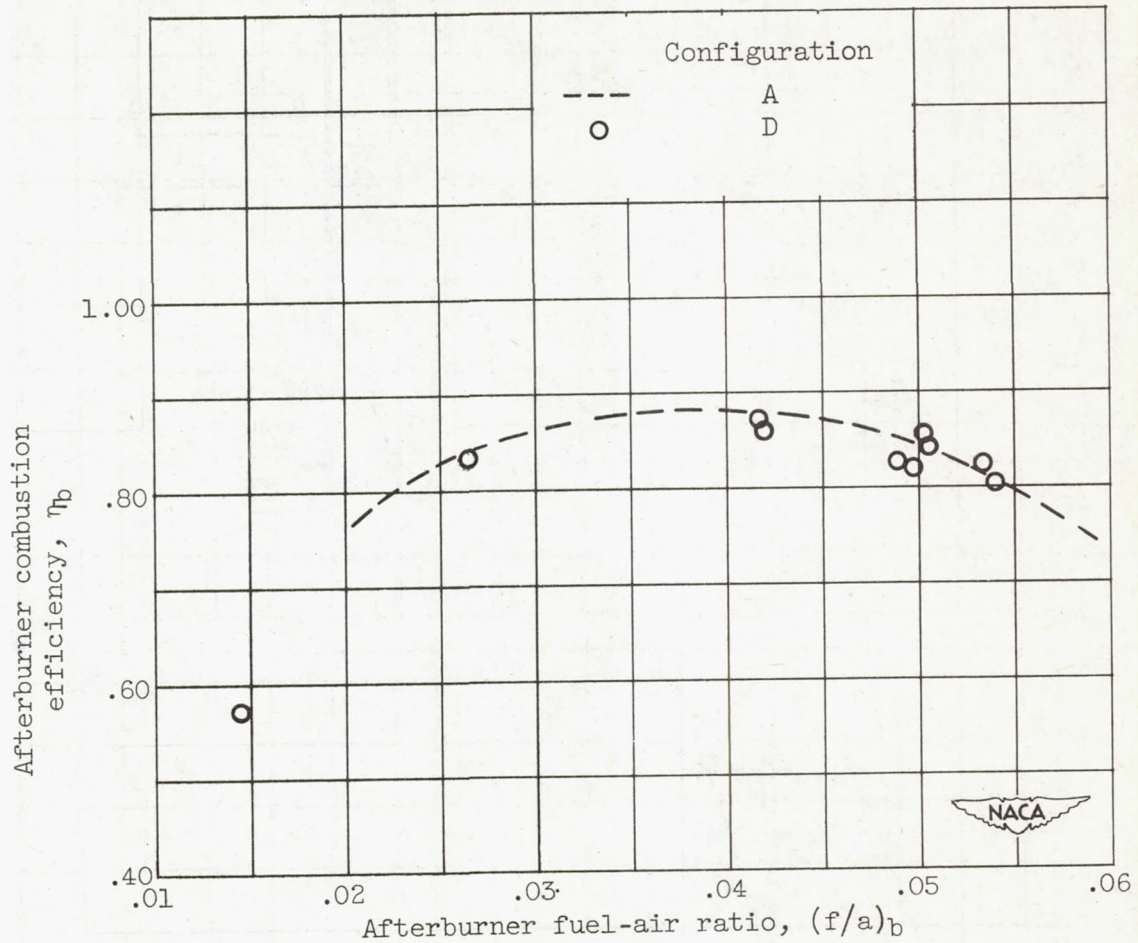
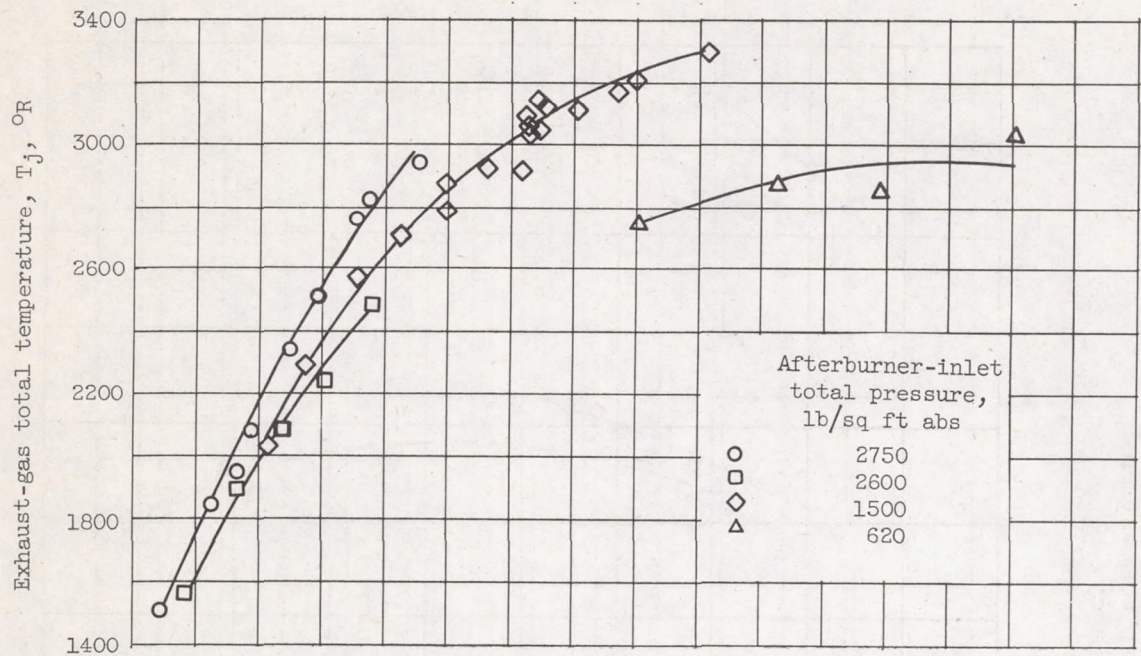
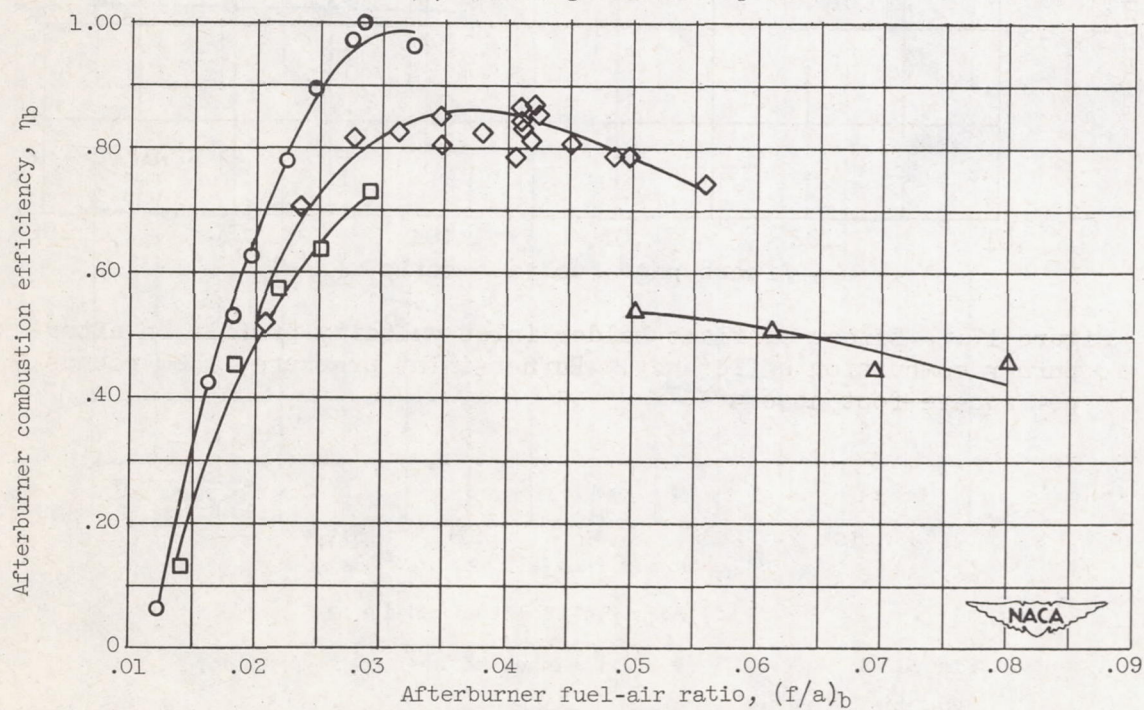


Figure 17. - Effect of flame-holder-inlet velocity profile on afterburner combustion efficiency. Burner-inlet pressure, 1500 pounds per square foot absolute.

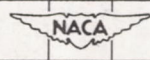


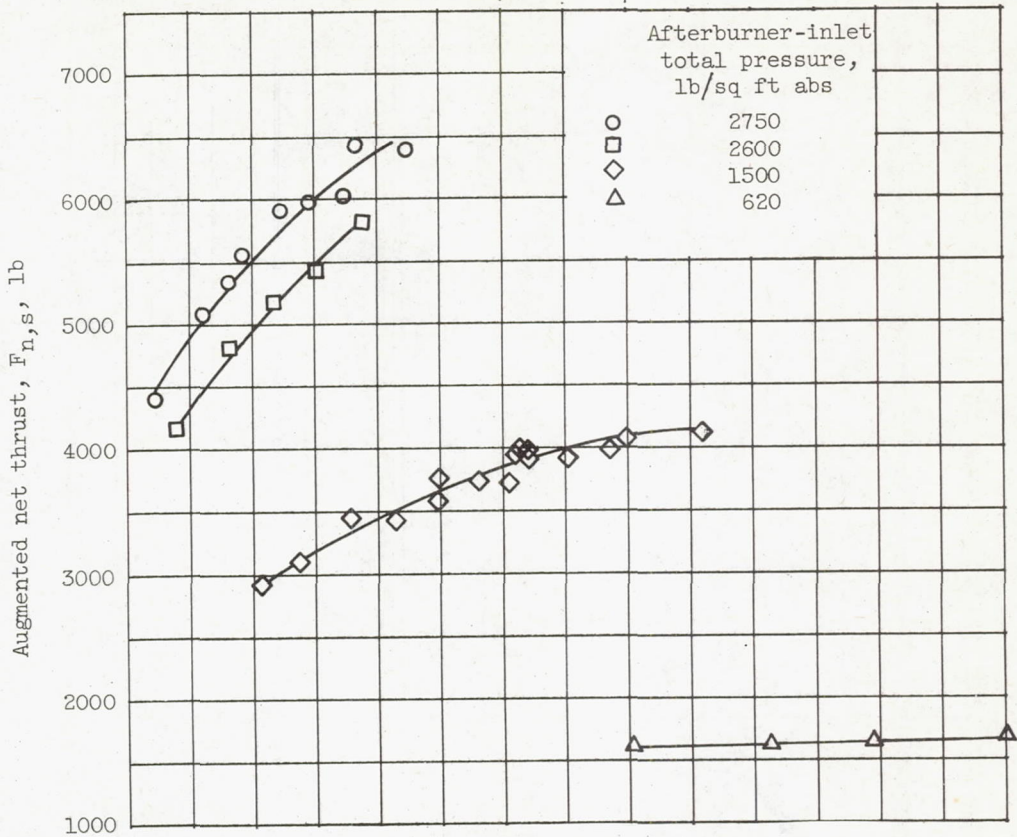
(a) Exhaust-gas total temperature.



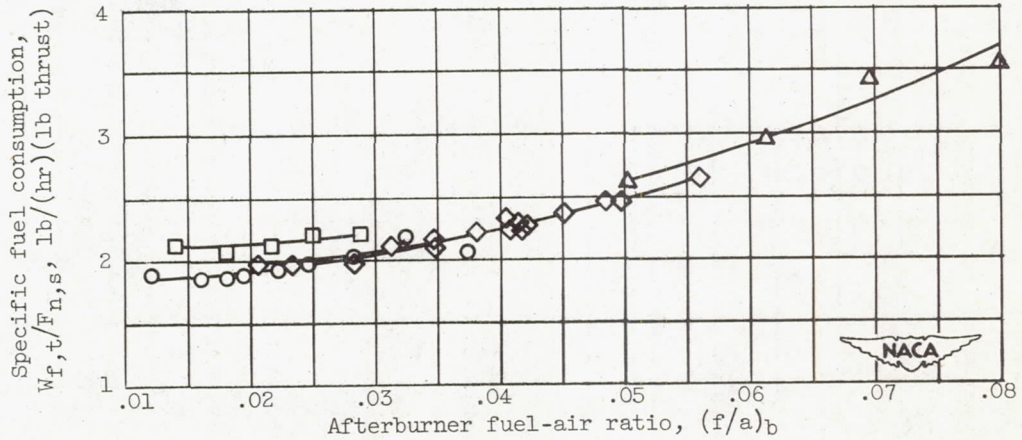
(b) Afterburner combustion efficiency.

Figure 18. - Performance of best configuration, H.





(c) Augmented net thrust.



(d) Specific fuel consumption.

Figure 18. - Concluded. Performance of best configuration, H.

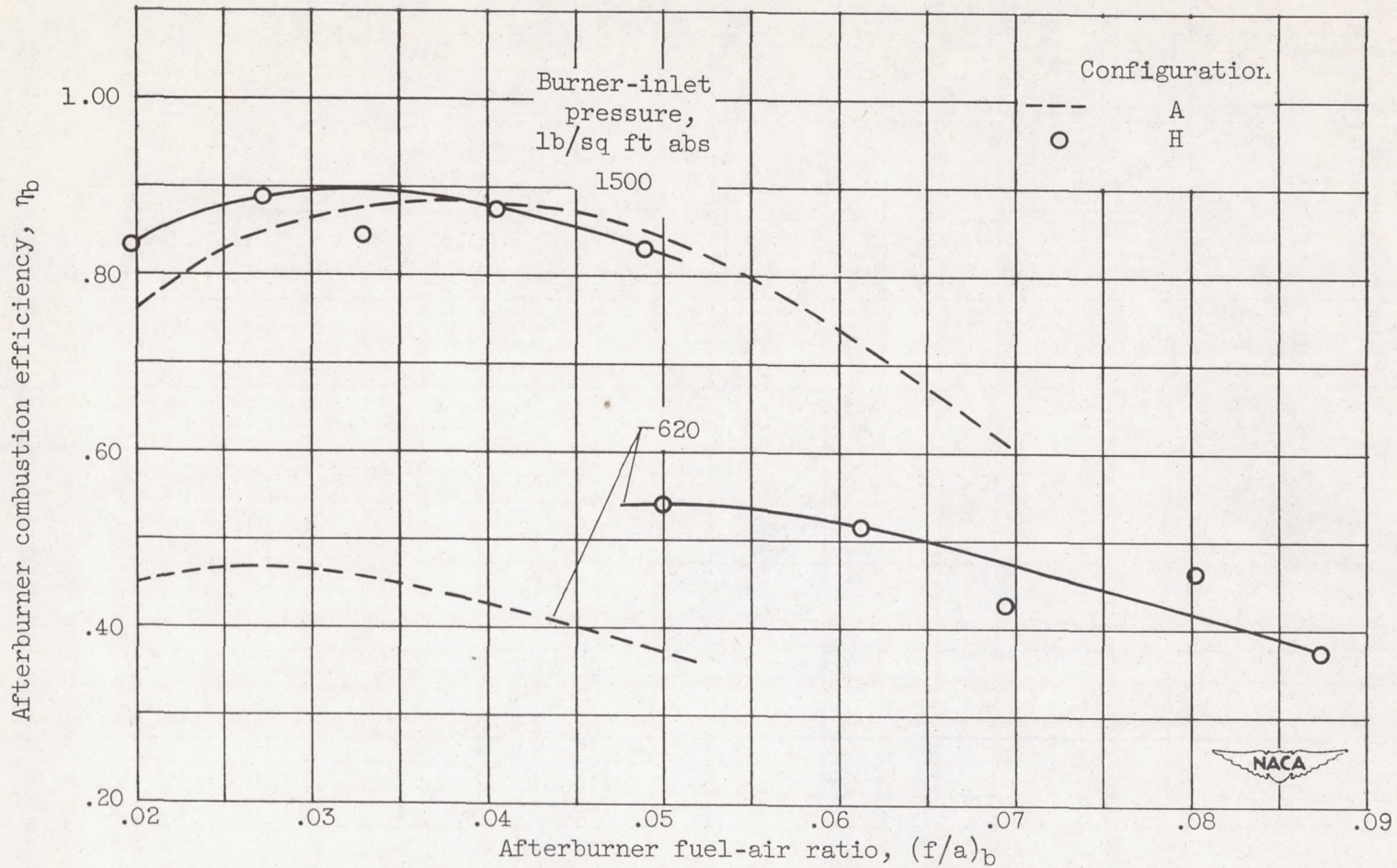


Figure 19. - Comparison of combustion efficiencies obtained with initial and best configurations.

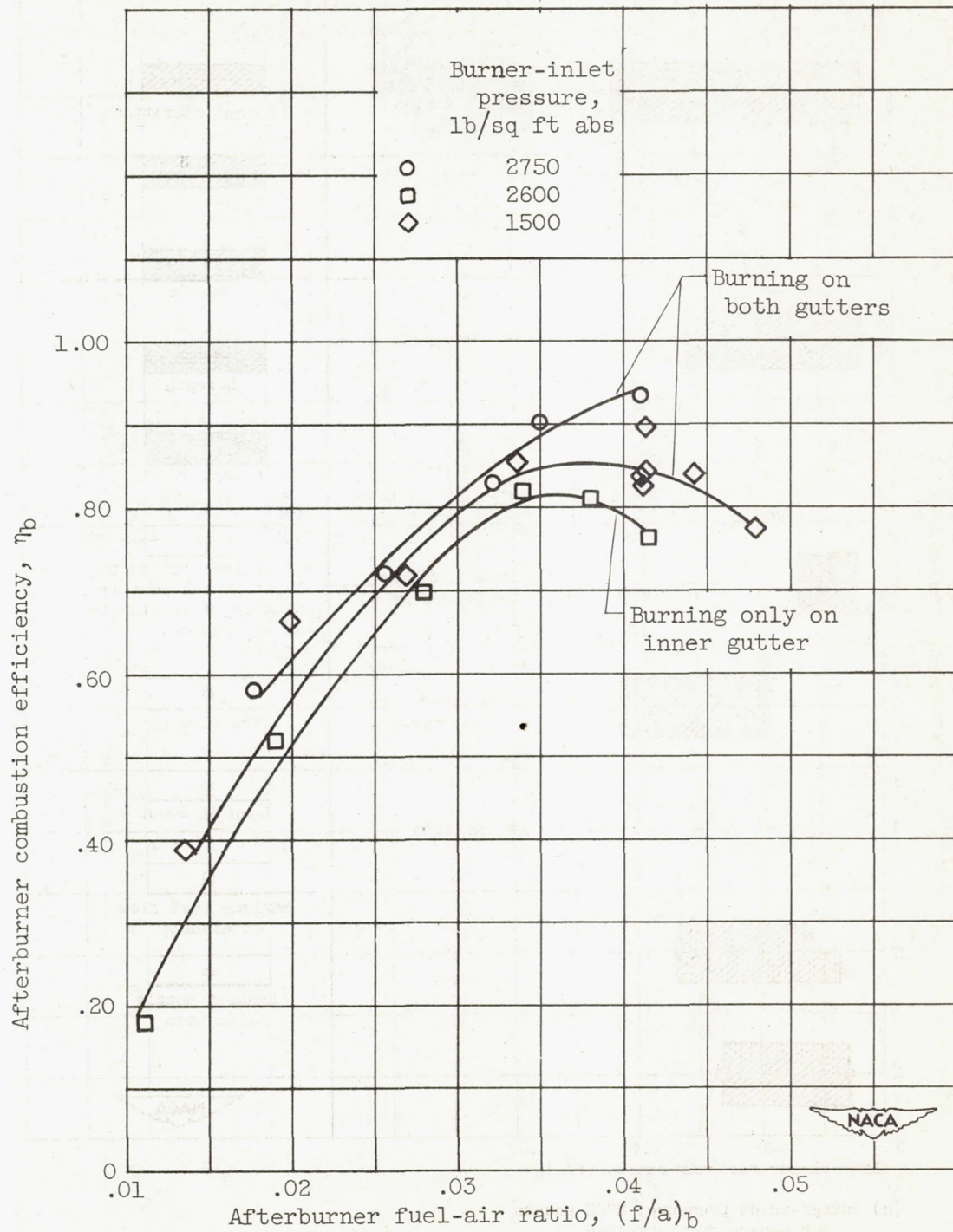
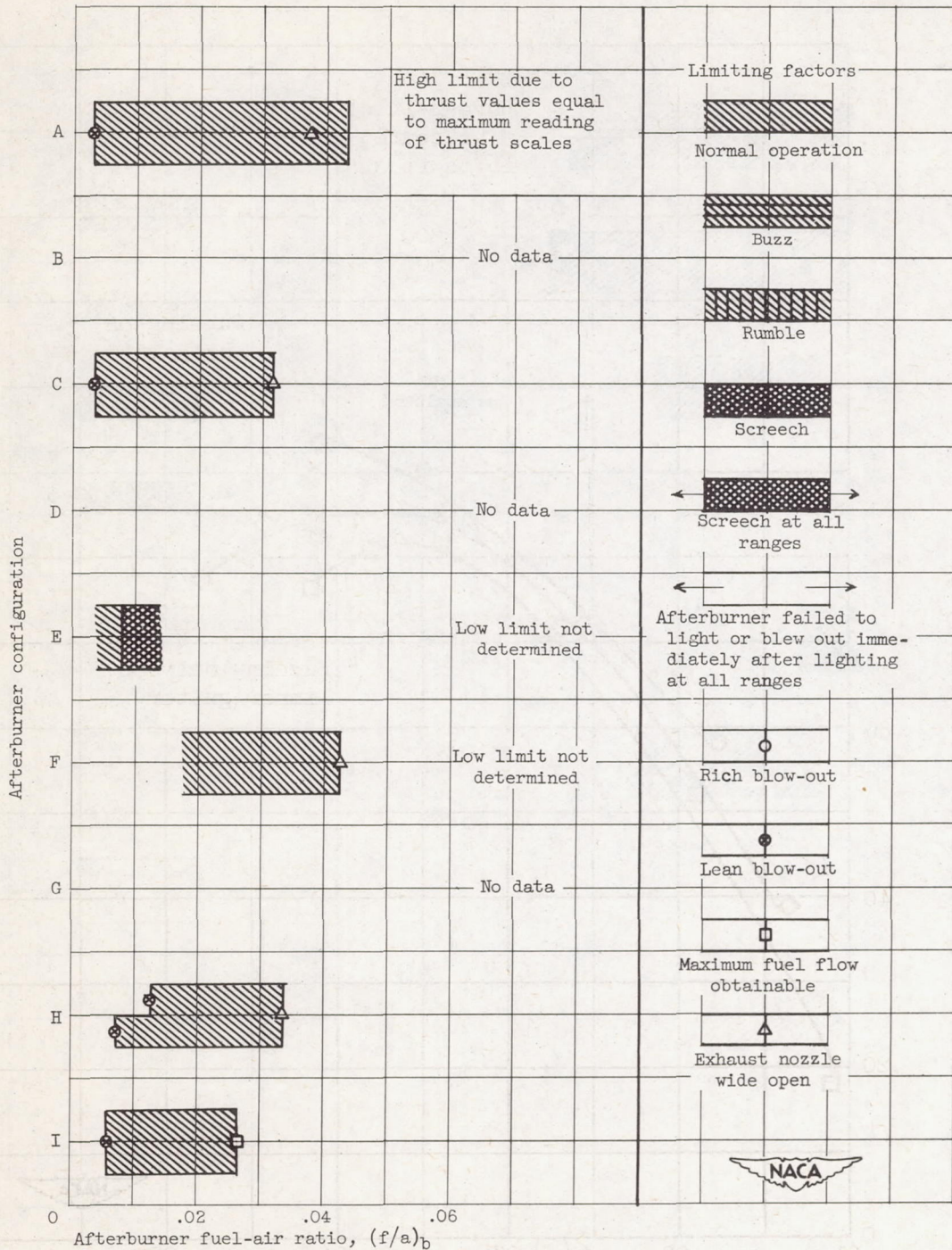
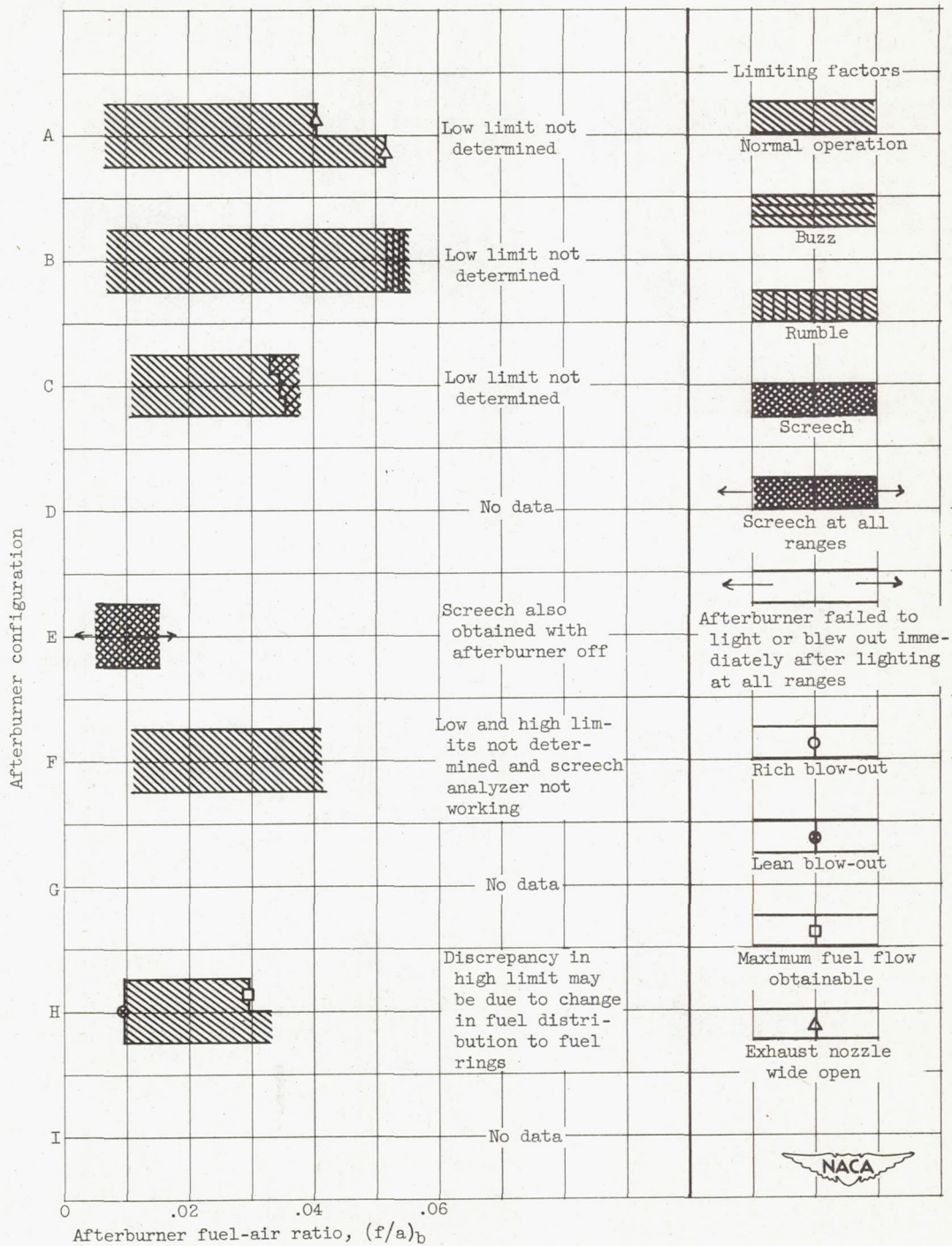


Figure 20. - Effect of faulty burning on combustion efficiency.



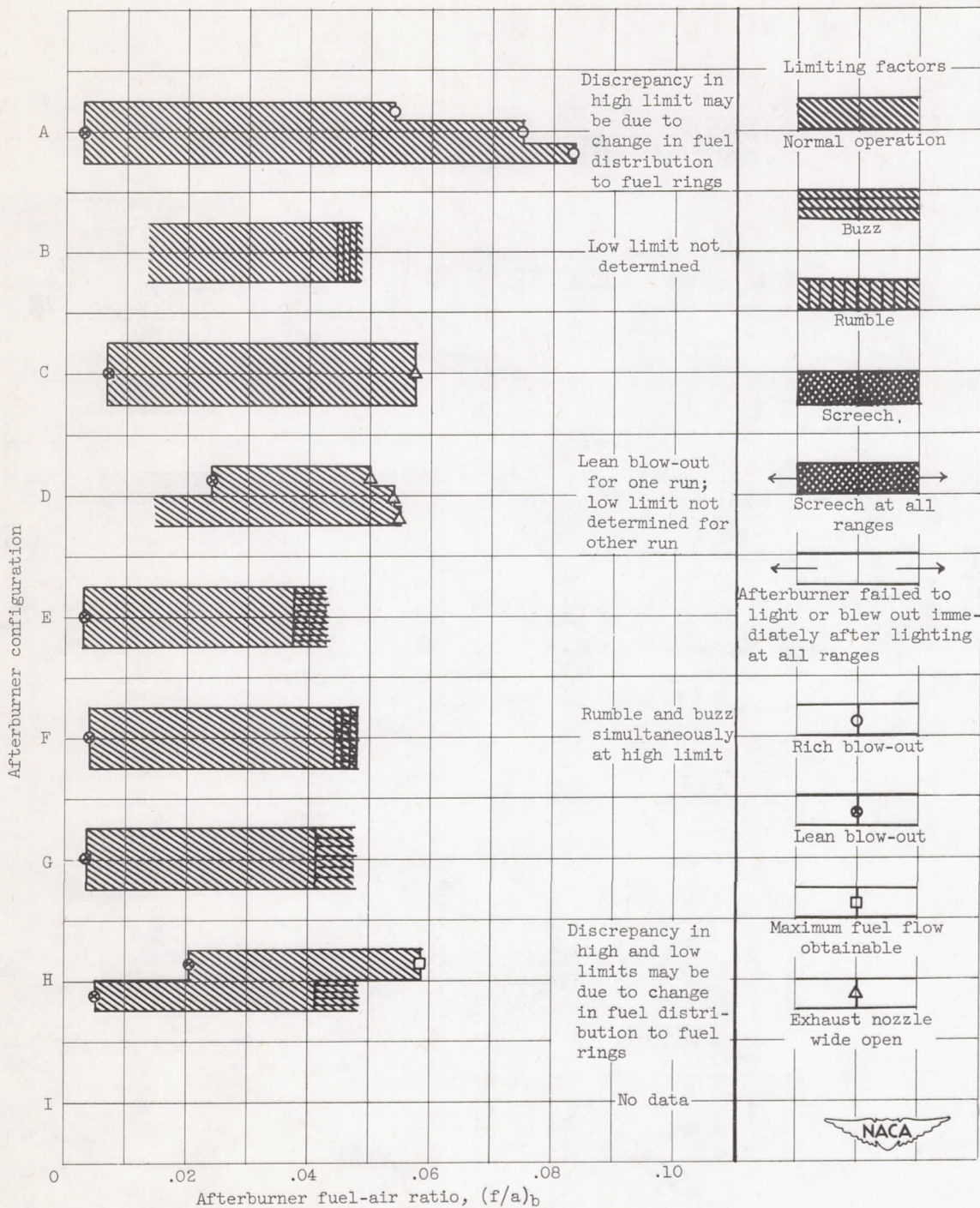
(a) Burner-inlet pressure, 2750 pounds per square foot absolute.

Figure 21. - Operational characteristics of all configurations.



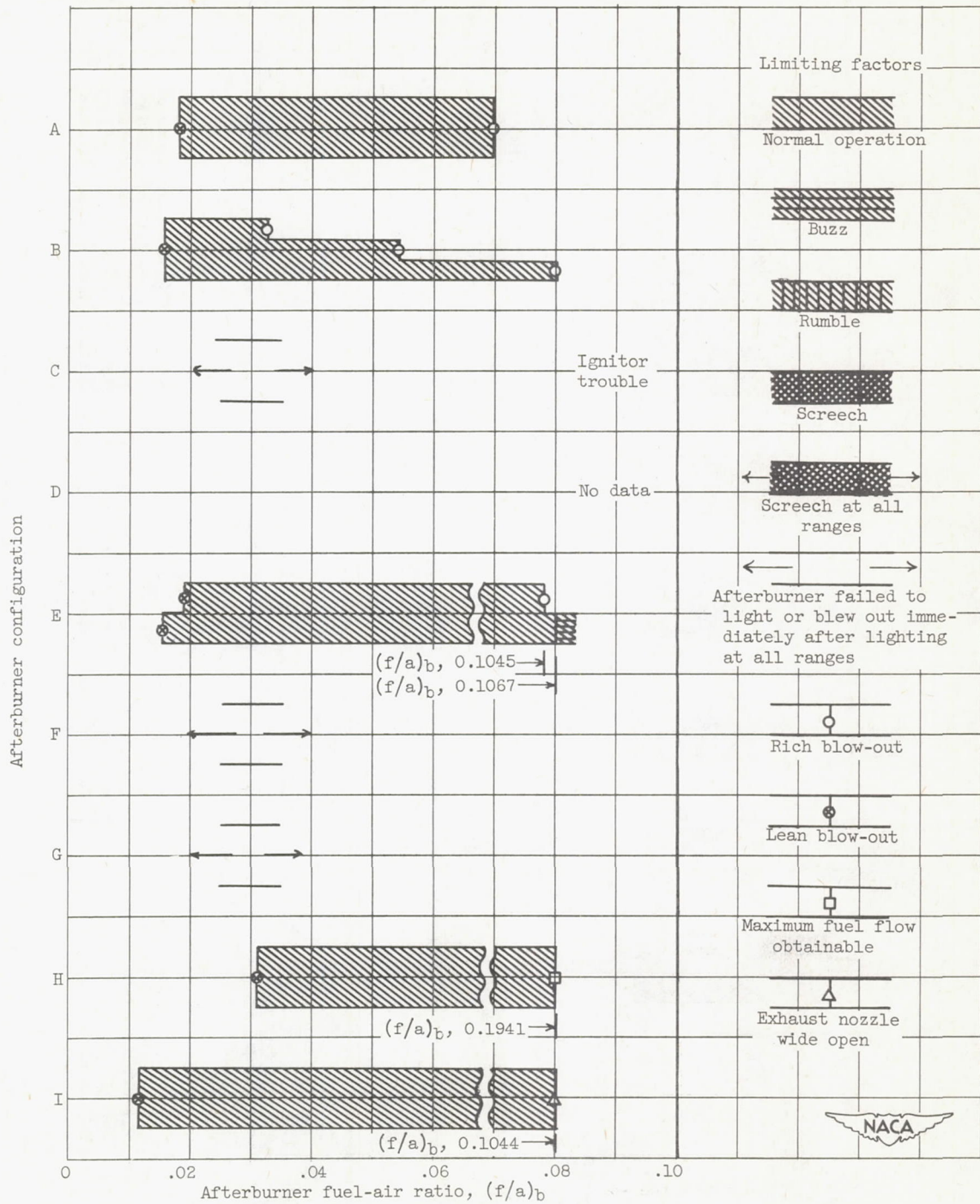
(b) Burner-inlet pressure, 2600 pounds per square foot absolute.

Figure 21. - Continued. Operational characteristics of all configurations.



(c) Burner-inlet pressure, 1500 pounds per square foot absolute.

Figure 21. - Continued. Operational characteristics of all configurations.



(d) Burner-inlet pressure, 620 pounds per square foot absolute.

Figure 21. - Concluded. Operational characteristics of all configurations.